

Reviewer #1

Reviewer comment: The authors discuss conjugate observations of two THEMIS satellites crossing the magnetopause in short succession, with ground based radar observations to determine the lengths of a dayside reconnection line at the magnetopause. The methodology seems to be interesting and the paper is well written with a very good introduction to the general problem. However I have some issues with the current data analysis and the event selection that are significant enough to not recommend publication at this time.

General Point: As the authors admit, their determined length of the X-line will be limited to the longitudinal coverage of the radars. This unavoidable limitation will always significantly influence their conclusion about the length of the “actual” X-line, which could be considerably longer, and will prevent them from ever finding a global answer. That will seriously limit the usefulness of the methodology, though generally its an interesting approach.

Response: We realize that the term “X-line extent” in our manuscript has caused confusion. The X-line the reviewer refers to is the magnetic geometry along which reconnection occurs at various rates and frequencies, which is indeed considerably longer than the radar coverage. However, our study intends to focus on the extent of reconnection bursts. We have revised the term “X-line extent” to “reconnection burst extent” as we do not aim at determining the extent of the global X-line but the localized bursty reconnection in the area of satellite-ground conjunction. Other bursts could occur outside the radar and satellite coverage but those are beyond the focus of this research. Please see also the response to the next comment.

With this clarification, the radar longitudinal coverage is sufficiently large for the purpose of this study. For example, the ionospheric flow structures under examination have a skewed Gaussian-shape velocity profile (Figures 2e, 5e, and 7e), and the FWHM of the profile is located completely within the radar coverage.

Reviewer comment: About the introduction: There are several significant publications using IMAGE/FUV observations. This mission had the ability to observe emissions from precipitating (cusp) ions over the entire polar region at once and was therefore not limited like the radar coverage in the present manuscript. Studies using these data have shown evidence that during southward IMF conditions the entire dayside is open leading to very long dayside reconnection lines. So, based on these results the length of the X-line is not the driving question. In additions, decades of cusp observations in all local time sectors show precipitating ions. X-lines in general seem to be very long. Cusp observations have shown that a substantial part of reconnection is dominated by pulsed reconnection [Lockwood et al., . . .]. The question is therefore – is the long X-line pulsing as “One” or are individual longitudinal sections have their own pulsation frequency? That should lead to scenarios presented in this manuscript, sections of X-lines that are active next to sections of X-lines temporarily inactive. This is how I would interpret the observations in the manuscript. Therefore the conclusion would not be about the length of the X-line since that would be masked by the temporal nature of the reconnection process, which might lead to misleading results.

In any case, I was surprised that there was no reference to this rather ground breaking IMAGE observations anywhere. These observations [e.g., Fuselier et al., 2002] should be added in the introduction and properly described.

Response: As the reviewer inferred we examine bursts of reconnection. Our study shows that a reconnection burst is not necessarily a pulse of a long X-line but can occur over a finite area.

IMAGE observations have provided global configuration of reconnection where reconnection bursts are embedded. The global-scale reconnection configuration is not the focus of this study but it offers valuable groundwork of clarifying the scope of the research. We rewrite the first paragraph as “...Reconnection tends to occur at sites of strictly anti-parallel magnetic fields as anti-parallel reconnection [e.g. Crooker, 1979; Luhmann et al., 1984], or occur along a line passing through the subsolar region as component reconnection [e.g. Sonnerup, 1974; Gonzalez and Mozer, 1974]. Evidence shows either or both can occur at the magnetopause and the overall reconnection extent can span from a few to 40 Re [Paschmann et al., 1986; Gosling et al., 1990; Phan and Paschmann, 1996; Coleman et al., 2001; Phan et al., 2001, 2003; Chisham et al., 2002, 2004, 2008; Petriner and Fuselier, 2003; Fuselier et al., 2002, 2003, 2005, 2010; Petriner and Fuselier, 2003; Pinnock et al., 2003; Bobra et al., 2004; Trattner et al., 2004, 2007, 2008, 2017; Trenchi et al., 2008]. However, reconnection does not occur uniformly across this configuration but has spatial variations [Pinnock et al., 2003; Chisham et al., 2008]. The local time extent of reconnection bursts is the focus of this study.”

Reviewer comment: Specific Points: Line 188: the D-shaped distribution do not persist into the ionosphere due to the conservation of the first adiabatic invariant. The D shape changes into a Crescent shape as soon as the ambient B field increases, which it definitely will in the cusps. This has been observed in the cusp regions for decades. This effect is so pronounced that it can be even used directly at the magnetopause. The “bending over” of the D-shape distribution observed during magnetopause crossings has been used in a recent study by Broll et al. (2017) (JGR) to determine the distance to the X-line from the MMS satellites and infer the X-line location.

Cusp Steps have nothing to do with D-shape distributions. Cusp steps are the result of changes in the reconnection rate at the magnetopause or caused by spatially separated X-lines. Cusp-steps have been discussed in great detail by Lockwood and Smith in the 90ties as manifestation of pulsed reconnection leading to the pulsed reconnection model and by e.g., Onsager et al [1995] or Trattner et al. [2002] as spatially separated X-lines.

Response: We agree with the reviewer and correct the statement as “The D-shaped ion distributions are deformed into a crescent shape as ions travel away from the reconnection site [Broll et al., 2017]”. We also replace case study #1 with a new event and the new event has a distorted D-shaped distribution. Details can be found below.

Reviewer comment: The authors use patchy reconnection also in the case of spatially separated X-line or partial X-lines. This will be a source of confusion for colleagues not too familiar with the subject. Patchy reconnection usually describes pulsed reconnection – temporal changes in reconnection. While the authors do a reasonable good job in trying to keep the temporal and spatial regimes apart I would recommend to revisit that issue throughout the paper.

Response: We follow the reviewer’s suggestion and add “the term patchy has also been used to describe the temporal characteristics of reconnection [e.g. Newell and Meng, 1991]. But this paper primarily focuses on the spatial properties”. We use “spatially patchy reconnection” to replace “patchy reconnection” throughout the text.

Reviewer comment: Figure 2: The symbol for Th-D is completely invisible – if it wasn’t for Figure 4 I would not have realized that there are indeed two separate magnetic foot points in that plot. Chose a different more prominent color.

Response: As advised by the reviewer we replace this event with an event that has good field line mapping. Please find the attachment for the new event.

Reviewer comment: Figure 2: it is mentioned in line 209 – the satellite foot points should map close to the radars FOV. I would recommend that the authors look for events where the satellite foot points are actually in the FOV of the radars to make absolutely sure that these observations are linked. Throughout the paper but especially in Figure 2 I do not have the impression that this is the case which makes the data analysis rather questionable. Therefore I fail to see how the observed D-shape distributions at the magnetopause are connected with particular flow channels which is the essential part of the study.

The authors also mark the cusp foot point in the radar images. Discussing again the events in figure 2, Th-D clearly saw an ion jet. It therefore observed reconnection at the magnetopause and was on a newly opened field line. The D shape distribution, while looking a bit crooked compared to the other D-shape distributions in the manuscript, travels along the magnetic field. The magnetic field, at that time the distribution was observed, was still northward. Therefore the satellite was in the LLBL and the ions move toward the northern cusp where the radar observations observe flow channels. All open magnetopause field lines map into the cusps. So the Th-D magnetic foot point, where the D-distribution was observed, should be in that region marked as cusp in figure 2d. It is not, it is not even in the FOV for the radar.

Response: To address reviewer's comment, we replace Figures 1-2 (see Figures 1-2). In the new event the footprint is within the radar FOV and close to the open-closed field line boundary. The corresponding text is changed to the following.

“3.1.1 In-situ satellite measurements

On February 2, 2013, THA and THE made simultaneous measurements of the dayside magnetopause with a 1.9 Re separation in the Y direction around 21:25 UT. The IMF condition is displayed in Figure 1a and the IMF was directed southward. The satellite location in the GSM coordinates is displayed in Figure 1b, and the measurements are presented in Figure 2. The magnetic field and the ion velocity components are displayed in the LMN boundary normal coordinate system, where *L* is along the outflow direction, *M* is along the X-line, and *N* is the current sheet normal. The coordinate system is obtained from the minimum variance analysis of the magnetic field at each magnetopause crossing [Sonnerup and Cahill, 1967]. Figures 2g-p show that both satellites passed from the magnetosheath into the magnetosphere, as seen as the sharp changes in the magnetic field, the ion spectra, and the density (shaded in pink).

As THE crossed the magnetopause boundary layer (2122:57-2123:48 UT), it detected both fluid and kinetic signatures of reconnection. It observed a rapid, northward-directed plasma jet within the region where the magnetic field rotated (Figures 2g and 2j). The magnitude of this jet relative to the sheath background flow reached 262 km/s at its peak, which was 72% of the predicted speed of a reconnection jet by the Walen relation (366 km/s, not shown). The angle between the observed and predicted jets was 39°. The ion distributions in Figure 2k showed a distorted D-shaped distribution similar to the finding of by Broll et al. [2018]. The distortion is due to particles traveling in the field-aligned direction from the reconnection site to higher magnetic field region, and Broll et al. [2018] estimated the traveling distance to be a few Re for the observed level of distortion.

THA crossed the magnetopause one to two minutes later than THD (2124:48-2125:13 UT). While it still identified a plasma jet at the magnetopause (Figures 2l and 2o), the jet speed was significantly smaller than what was predicted for a reconnection jet (80 km/s versus 380 km/s in the *L* direction).

The observed jet was directed 71° away from the prediction. The ion distributions deviated from clear D-shaped distributions (Figure 2p). Reconnection was thus much less active at THA local time than at THE. This suggests that the X-line of the active reconnection at THE likely did not extend to THA.

3.1.2 Ground radar measurements

The velocity field of the dayside cusp ionosphere during the satellite measurements is shown in Figures 2a-c. Figure 2a shows the radar LOS measurements at 21:25 UT, as denoted by the color tiles, and the merged vectors, as denoted by the arrows. The colors of the arrows indicate the merged velocity magnitudes, and the colors of the tiles indicate the LOS speeds that direct anti-sunward (those project to the sunward direction appear as black). Fast (red) and anti-sunward flows are the feature of our interest. One such of this flow can be identified in the pre-noon sector, which had a speed of ~ 800 m/s and was directed poleward and westward. As the merged vector arrows indicate, the velocity vectors have a major component close to the INV beam directions and thus the INV LOS velocities reflect the flow distribution. The flow crossed the open-closed field line boundary, which was located at 78° MLAT based on the spectral width (Figure 2d and S1). This flow thus meets the criteria of being an ionospheric signature of magnetopause reconnection. Another channel of fast flow was present in the post-noon sector. This post-noon flow was directed more azimuthally and was separated from the pre-noon flow by a region of slow velocities at $>79^\circ$ MLAT around noon. The two flows are thus two different structures likely originating from two discontinuous reconnection bursts. Since the satellites were located in the pre-noon sector we focus on the pre-noon flow below.

The flow had a limited azimuthal extent. The extent is determined at half of the maximum flow speed, which was ~ 400 m/s. Figure 2f discussed below shows a more quantitative estimate of the extent. In Figure 2a, we mark the eastern and western boundaries with the dashed magenta lines, across which the LOS velocities dropped from red to blue/green colors.

Figure 2b shows the SECS velocities, denoted by the arrows. The SECS velocities reasonably reproduced the spatial structure of the flows seen in Figure 2a. The flow boundaries were marked by the dashed magenta lines, across which the flow speed dropped from red to blue. Across the flow western boundary the flow direction also reversed. The equatorward-directed flows are interpreted as the return flow of the poleward flows, as sketched in Southwood [1987] and Oksavik et al. [2004].

The velocity field reconstructed using the SHF velocities is shown in Figure 2c (obtained through the Radar Software Toolkit (<http://superdarn.thayer.dartmouth.edu/software.html>)). This is an expanded view of the global convection maps in Figure S2 focusing on the dayside cusp and the employed radars listed in Section 2 have contributed to the majority of the backscatters on the dayside. The SHF velocities also captured the occurrence of two flows in the pre- and post-noon sectors, respectively, although the orientation of the flows were less azimuthally-aligned than Figure 2a or 2b. The difference is likely due to the contribution from the statistical potential distribution under the southward IMF. The flow western and eastern boundaries were again marked by the dashed magenta lines.

Figure 2d shows spectral width measurements. Large spectral widths can be produced by soft (~ 100 eV) electron precipitation [Ponomarenko et al., 2007] such as cusp/mantle precipitation, and evidence has shown that the longitudinal extent of large spectral widths correlates with the extent of PMAFs [Moen et al., 2000] and of poleward flows across the OCB [Pinnock and Rodger, 2001]. Large spectral widths thus have the potential to reveal the reconnection burst extent. For the specific event under examination, the region of large spectral widths, appearing as red color, spanned from 10.5 to 14.5 h MLT if we count the sporadic scatters in the post-noon sector. This does not contradict the flow width identified above because the wide width reflects the summed width of the pre- and post-noon flows. In fact a more careful examination shows the presence of two dark red (>220 m/s spectral width) regions

embedded within the ~ 200 -m/s spectral widths (circled in red, the red dashed line is due to the discontinuous backscatters outside the INV FOV), corresponding to the two flows.

Figures 2a-c all observed a channel of fast anti-sunward flow in the pre-noon sector of the high latitude ionosphere, and the flow had a limited azimuthal extent. If the flow corresponded to magnetopause reconnection, the X-line is expected to span over a limited local time range. This is consistent with the THEMIS satellite observation in Section 3.1.1, where THE at $Y = -2.9$ Re detected clear reconnection signatures, while THA at $Y = -4.8$ Re did not. In fact, if we project the satellite location to the ionosphere through field line tracing under the T89 model, THE was positioned at the flow longitude, while THA outside the flow was to the west (Figure 2a).

While this paper primarily focuses on the spatial extent of reconnection bursts, the temporal evolution of reconnection can be obtained from the time series plot in Figure 2e. Figure 2e presents the INV LOS measurements along 80° MLAT (just poleward of the open-closed field line boundary with good LOS measurements) as functions of magnetic longitude (MLON) and time. Similar to the snapshots, the color represents LOS speeds that project to the anti-sunward direction, and the flow of our interest appears as a region of red color. The time and the location where THA and THE crossed the magnetopause are marked by the vertical and horizontal lines. The flow emerged from a weak background at 2120 UT and persisted for ~ 30 min in INV FOV. At the onset the flow eastern boundary was located at -82° MLON, and interestingly, this boundary spread eastward with time in a similar manner as events studied by Zou et al. [2018]. The flow western boundary was located around -77° MLON during 2120-2134 UT, and started to spread eastward after 2134 UT. Hence the reconnection-related ionospheric flow, once formed, has spread in width and displaced eastward. The spreading has also been noticed in the other two events (see Section 3.3), indicating that this could be a common development feature of the reconnection-related flows. The spreading was fast in the first 6 min and then slowed down stabilizing at a finite flow extent (until the eastern boundary went outside FOV at 2134 UT).

A consequence of the flow temporal evolution is that THA, which was previously outside the reconnection-related flow, became immersed in the flow from 2130 UT, while THE, which was previously inside the flow, was left outside from 2142 UT (Figure 2e). This implies that at the magnetopause the reconnection has spread azimuthally sweeping across THA, and has slid in the $-y$ direction away from THE. This is in perfect agreement with satellite measurements shown in Figures 2q-z. Figures 2q-z presents subsequent magnetopause crossings made by THA and THE following the crossings in Figures 2g-p. THA detected an Alfvénic reconnection jet and a clear D-shape ion distribution, and THE detected a jet much slower than the Alfvénic speed and an ion distribution without a clear D-shape. This corroborates the connection between the in-situ reconnection signatures with the fast anti-sunward ionospheric flow, and reveals the dynamic evolution of reconnection in the local time direction.

We quantitatively determine the flow extent in Figure 2f. Figure 2f shows the INV LOS velocity profile at 2125 UT as a function of magnetic longitude and distance from 0° MLON. The 2125 UT is the same time instance as in Figures 2a-c and is the time when the flow extent has slowed down from spreading and stabilized. The profile is taken along 80° MLAT. While this latitude is 2° poleward of the open-closed field line boundary, the shape of the flow did not change much over the 2° displacement and thus still presents the reconnection extent. The flow velocity profile has a skewed Gaussian shape, and we quantify the flow azimuthal extent as the full-width-at-half-maximum (FWHM). The FWHM was 13° in MLON or 260 km at an altitude of 260 km. Also shown is the SECS velocity profile. Here we only show the northward component of the SECS velocity as this component represents reconnecting flows across an azimuthally-aligned open-closed field line boundary. The SECS velocity profile gives

a FWHM of 13.5° in MLON or 270 km, very similar to the LOS profile.

It is noteworthy mentioning that the velocity profile obtained above approximates to the profile of reconnection electric field along the open-closed field line boundary (details in Figure S3). Reconnection electric field can be estimated by measuring the flow across the open-closed field line boundary in the reference frame of the boundary [*Pinnock et al.*, 2003; *Freeman et al.*, 2007; *Chisham et al.*, 2008]. However, a precise determination of the boundary motion is subject to radar spatial and temporal resolution and for a slow motion like events studied in this paper (Figure S1), the signal to noise ratio is lower than one. For this reason this paper focuses on the velocity profile poleward of the open-closed field line boundary, which is less affected by the error associated with the boundary. To infer the reconnection extent at the magnetopause, we project the flow width in the ionosphere to the equatorial plane. The result suggests that the reconnection local time extent was ~ 3 Re.

Before closing this section, we would like to point out that the determined extent is characterized by the FWHM of the fast anti-sunward ionospheric flow, which allows weak flows to extend beyond the flow extent. When THA and THE were positioned within the weak flows in the ionosphere, they at the magnetopause observed flows much weaker than the Walen prediction. This may imply that there were two components of reconnection at different scales in this event: weak background reconnection signified by the slow flows, and embedded strong reconnection bursts signified by the fast flows.”

Reviewer comment: Line 338: One of the open questions in magnetic reconnection is still how the reconnection rate develops along the length of the X-lines. Since decades of research showed that pulsed reconnection is a rather significant process, it is conceivable that individual sections along a “long” X-line pulse at different frequencies. I therefore would expect that it is very likely that magnetopause crossings by multiple satellites show active and temporarily inactive sections along an X-line. This is not prove that a dayside X-line is short. The interpretation of the authors that this event is a spatially restricted X-line based on flow channels at very different latitudes is not convincing, especially since the satellite observations are outside the flow channels for which observations exist. I also want to stress that in the pulsed reconnection model, field lines that were opened before reconnection briefly stopped, are convecting and provide a continuous transfer of magnetosheath plasma into the magnetosphere. That should certainly influence your radar observations. It is unlikely that the ionosphere would respond that quickly to short changes in the reconnection rate. The magnetosphere is generally rather slow in its response to outside changes. That will make linking ionospheric flow channels to magnetopause observations rather challenging. Radar observations of ionospheric convection, direction and velocities, are often used to estimate global convection pattern in the polar ionosphere using various models. These “convection cells” could be overlaid in the radar plots to make a connection between the satellite magnetic foot points outside the radar FOV and the radar data. Depending on how these global convection cells look like they might provide a more convincing picture that these observations are actually linked.

Response: We have replaced Figures 1-2 to the new event where the satellite footprints were within the radar FOV and close to the open-closed field line boundary. We believe that this event provides a more convincing case for establishing the space and ground connection.

We agree with the reviewer that reconnection can happen over various temporal scales but the typical time scale of reconnection bursts, or FTEs is found to be a few minutes [*Lockwood and Wild*, 1993; *Kuo et al.*, 1995; *Fasel*, 1995]. This can be resolved by radars considering that M-I coupling time scale on the dayside is $\sim 1-2$ min [e.g. *Carlson et al.*, 2004]. Studies have compared the time scale of

ionospheric flows with FTEs and found a very similar distribution [McWilliams et al., 1999], suggesting that ionospheric flows well capture reconnection variability at least down to FTE time scale. We add the following text to the end of the methodology section.

“Note that reconnection can happen over various spatial and temporal scales and our space-ground approach can resolve reconnection bursts that are larger than $0.5 R_e$ and persist longer than a few minutes. This is limited by the radar spatial and temporal resolution, and the magnetosphere-ionosphere coupling time which is usually 1-2 min [e.g. Carlson et al., 2004]. This constraint is not expected to impair the result because reconnection bursts above this scale have been found to occur commonly in statistics (see the Introduction section for spatial and Lockwood and Wild [1993], Kuo et al. [1995], Fasel [1995], and McWilliams et al. [1999] for temporal characteristics).”

We have followed the reviewer’s opinions and added the global convection pattern in supporting Figure S2. The radars employed in the paper has contributed to the majority of the backscatter on the dayside and including more radars do not change the conclusion. Again we focus on the extent of individual reconnection-related flow, not the sum of all the flows on the dayside. It may also noteworthy to point out an important difference between our study and previous studies: our events occurred under non-storm time, where the open-closed field line is confined within the utilized few radar FOVs, while previous studies using a wider network of SuperDARN radars focus on storm time period where the boundary has expanded to low latitude.

Reviewer #2

This paper is concerned with estimating the extent of reconnection X-lines on the Earth's magnetopause, with an overall aim of measuring, and understanding spatial and temporal variability in magnetic reconnection. For studies of this type, conjugate observations combining spacecraft and ground-based measurements can be very important. There are some aspects of reconnection (such as the localised plasma physics) that can only be measured by in-situ spacecraft. There are also some aspects (such as the macrophysics of the process) that can only be measured by instruments that provide a wider view, such as auroral imagers or ground-based radars. However, the local time extent of reconnection regions can only be determined unambiguously using ionospheric measurements (in the absence of a massive armada of spacecraft). Similarly, the amount of flux transfer occurring during reconnection can only be determined unambiguously using ionospheric measurements. And consequently, the patchy (spatial variation) and bursty (temporal variation) of reconnection can only be unambiguously studied using ionospheric measurements.

To measure the extent of reconnection from ionospheric measurements (which can then be mapped back to the magnetopause) first requires the identification of the ionospheric footprint of the open-closed magnetic field line boundary (OCB). The regions where the ionospheric plasma flow crosses this boundary (in the frame of the boundary – which is typically in motion itself) map to the regions on the magnetopause where reconnection is occurring. Although the text shows that the authors appear to appreciate this, they do not analyse their ionospheric data in this way.

Consequently, I have some major issues with the introductory text and the radar data analysis and presentation. The authors need to address these major points before the paper can be reviewed properly.

(1) Some of the background referencing is misdirected and inadequate:

The referencing of spacecraft observations associated with reconnection (extending from lines 95 to 117) starts with the phrase – ‘The extent of reconnection X-lines has been observationally determined based on fortuitous satellite conjunctions. . .’. This is not true. Even if the word ‘determined’ was changed to ‘estimated’ it would still be a stretch of the truth. The ‘extent of reconnection X-lines’ cannot be unambiguously determined (or even estimated) from spacecraft observations. Interpretations of multiple spacecraft observations still have to make the assumption that the X-line is continuous between spacecraft, or that it is not continuous between spacecraft. X-lines may also continue longitudinally outside of the view of the spacecraft. All that multiple spacecraft measurements can do (given that the assumptions made are correct) is provide upper or lower limits on the X-line extent.

Response: We completely agree with the reviewer's opinion on the limitations of spacecraft observations. Those limitations are the exact motivation of adopting the space-ground approach in this paper as mentioned in the introduction section. We change the statement to “studies have attempted to constrain the extent of reconnection X-lines based on fortuitous satellite conjunctions”. The word “constrain” has been used by the paper “Spacecraft measurements constraining the spatial extent of a magnetopause reconnection X line” by Walsh et al. 2017.

The referencing of ionospheric observations associated with reconnection (extending from lines 118 to 141) concentrates on those related mainly to local (often single radar) measurements of fast anti-sunward flows observed by radar (such as pulsed ionospheric flows [PIFs]) and their auroral counterpart (poleward-moving auroral forms [PMAFs]). These typically occur within the polar cap, and not necessarily at the ionospheric footprint of the OCB. Although all these observations are of phenomena that are consequences of reconnection, and which provide important information about the patchy and bursty nature of reconnection (and links to FTEs, etc.), they don't allow the unambiguous estimation of the extent of the X-line. Hence, many of these references are actually

superfluous to the paper. As mentioned above, to measure the extent of the reconnection X-line in the ionosphere requires the identification of the footprint of the OCB and the region for which there is plasma flow across it. (Although, similar caveats to the spacecraft observations also exist if there is not complete longitudinal coverage covering the whole ionospheric projection of the X-line.) There are a large number of papers that have studied and measured reconnection in this way that are not mentioned in the introduction of the present paper. A significant reference that reviews most of the work in this area, as well as outlining the techniques required to make these measurements, is Chisham et al. (2008) – Remote sensing of the spatial and temporal structure of magnetopause and magnetotail reconnection from the ionosphere – *Rev. Geophys.*, 46, RG1004. Other papers that have measured the extent of the reconnection X-line using these methods include; (i) Pinnock et al. (2003) – The location and rate of dayside reconnection during an interval of southward interplanetary magnetic field – *Ann. Geophys.*, 21, 1467-1482, which studied the same event that was observed in Equator-S data by Phan et al. (2000). They estimated the length of the reconnection X-line on the dayside magnetopause at this time to be ~ 38 Re based on the 10 hours of local time that flow was observed crossing the OCB in the ionosphere. (ii) Chisham et al. (2004) – Measuring the dayside reconnection rate during an interval of due northward interplanetary magnetic field – *Ann. Geophys.*, 22, 4243-4258, which measured the X-line extent of lobe reconnection during northward IMF to be ~ 6 -11 Re.

Response: We thank the reviewer for the important references. We realize that the term “X-line extent” in our manuscript has caused confusion. In our original terminology we used “magnetic separator” to refer to the global configuration along which reconnection occurs at various rates, and used “X-lines” to refer to regions of strong reconnection, i.e., reconnection bursts. Such usage has been common in the literature (especially in FTE studies [e.g., Fear et al., 2008, 2010] and local numerical simulations [e.g., Shay et al., 2003; Sheperd and Cassak, 2012]). But to avoid confusion we replace “extent of X-lines” with “extent of reconnection bursts” throughout the text. Therefore the title of the paper is “local time extent of magnetopause reconnection bursts using space-ground coordination”. Similar changes are made throughout the text.

The references suggested by the reviewer provide valuable groundwork of clarifying the scope of this study. We rewrite the first paragraph as
“...Reconnection tends to occur at sites of strictly anti-parallel magnetic fields as anti-parallel reconnection [e.g. Crooker, 1979; Luhmann et al., 1984], or occur along a line passing through the subsolar region as component reconnection [e.g. Sonnerup, 1974; Gonzalez and Mozer, 1974]. Evidence shows either or both can occur at the magnetopause and the overall reconnection extent can span from a few up to 40 Re [Paschmann et al., 1986; Gosling et al., 1990; Phan and Paschmann, 1996; Coleman et al., 2001; Phan et al., 2001, 2003; Chisham et al., 2002, 2004, 2008; Petrinec and Fuselier, 2003; Fuselier et al., 2002, 2003, 2005, 2010; Petrinec and Fuselier, 2003; Pinnock et al., 2003; Bobra et al., 2004; Trattner et al., 2004, 2007, 2008, 2017; Trenchi et al., 2008]. However, reconnection does not necessarily occur uniformly across this configuration but has spatial variations [Pinnock et al., 2003; Chisham et al., 2008]. The local time extent of reconnection bursts is the focus of this study.”

(2) Identification of the extent of the reconnection region from fast ionospheric flows is flawed: Lines 52-54 state – ‘The extent has also been inferred by radars as fast ionospheric flows moving anti-sunward across the open-closed field line boundary, but whether a particular ionospheric flow results from reconnection needs to be confirmed.’ Firstly, the measured flows do not need to be fast. The fast flows highlighted in the paper are obviously driven by

reconnection but these are predominantly polar cap flows (relating to the newly-opened flux tubes moving over the polar regions towards the nightside), not flows at and across the OCB. Any flow across the OCB, whether fast or slow, implies that reconnection has occurred, as closed flux has been converted to open flux. By the same argument, if flow across the OCB is measured, spacecraft measurements are not required to prove that this flow is a result of reconnection (hence I disagree with the statement on lines 132-135).

Lines 198-206 detail the SuperDARN radars used in the study. What I do not understand is why the authors restricted their study to only a few of the northern hemisphere radars when there is a much wider network of northern hemisphere SuperDARN radars that would provide a much greater longitudinal coverage? Larger coverage provides a much better global picture of the ionospheric convection and hence the reconnection driven flows across the OCB.

Response: We agree that conceptually ionospheric flows moving across the OCB, even slow, should be related to reconnection. However, to the best of our knowledge, there has been no confirmation of whether weak ionosphere flows meet the quantitative in-situ magnetopause reconnection criteria and our event #1 (updated as seen in the attachment) suggests that they actually correspond to plasma jets at the magnetopause much slower than the Alfvén speed. Thus the slow ionospheric flows do not meet the in-situ definition of reconnection but should be treated separately. The focus of this paper is on strong bursts of reconnection. But our study, as well as Chisham et al. [2008], may have suggested that there are two components of reconnection at different scales: weak background reconnection signified by the slow flows, and embedded strong reconnection bursts signified by the fast flows.

To avoid confusion, we replace the sentence as “The validity of the assumption can be tested by radars via examining ionospheric flows moving anti-sunward across the open-closed field line boundary”.

The PolarDARN radars utilized in the paper have provided sufficient coverage for studying reconnection bursts in the area of satellite-ground conjunction. Reconnection bursts may also activate outside the radar FOV, but those are not the focus of the satellite-ground conjunction study and the terminology change mentioned above clarifies that this paper is not meant to determine the global X-line extent but individual reconnection burst extent. Backscatters from radars at lower latitudes were limited (see Figure S2) because the cusp, and the associated ionospheric irregularities, occurred at relatively high latitude ($>77-78^\circ$ MLAT). It is noteworthy to point out the studied events occurred under non-storm time, while previous studies using a wide network of SuperDARN radars focus on storm time period where the OCB has expanded to low latitude.

Lines 297-298 state – ‘The extent is determined at half of the maximum flow speed, which was ~ 400 m/s’. Why? There is still flow across the boundary outside this region that results from reconnection. Consequently, the dashed magenta lines in figures 2, 4, and 6 mean nothing, except to nicely frame the fast poleward flows into the polar cap. In a similar vein, lines 366-367 state ‘We quantify the flow azimuthal extent as the full-width-at-half-maximum (FWHM) of the velocity profile’. Why? Any poleward flow (across the OCB) represents the creation of newly reconnected flux. In all 3 examples there are significant poleward flows east of the dashed magenta lines. In figures 2e and 2f the flow extent is ‘quantitatively determined’ using measurements at 80 degrees latitude. Why use the flows at this latitude to determine the longitudinal extent when they are well within the polar cap? These are not the same as the

flows at the OCB latitude, and hence they do not show the longitudinal extent of reconnection. Hence, they cannot be reliably used to estimate the length of the X-line.

Response: We appreciate the reviewer's comment. As clarified above, we focus on reconnection bursts, which appear as fast anti-sunward flows in the ionosphere. It has been a common approach to measure the reconnection burst extent as the flow extent at a latitude poleward of the OCB [Goertz et al., 1985; Pinnock et al., 1993, 1995; Provan and Yeoman, 1999; Thorolfsson et al., 2000; McWilliams et al., 2001a, 2001b; Elphic et al., 1990; Denig et al., 1993; Neudegg et al., 1999, 2000; Lockwood et al., 2001; Wild et al., 2001, 2003, 2007; McWilliams et al., 2004; Zhang et al., 2008]. Slow flows have been allowed to extend beyond the boundaries of the fast flows [McWilliams et al., 2004], and we have clarified how fast and slow ionosphere flows are contrasted in terms of in-situ flows above. Since the longitudinal profile of the flow velocity has a skewed Gaussian shape, we have used FWHM. The use of FWHM is analogous to the methodology of Shay et al. [2003], who define reconnection as regions where the current density is larger than half of what is carried by the electron Alfvén speed. This is clarified in the text.

We have compared our flow velocity profile with the reconnection electric field at the OCB in Figure S3. Figures S3a-c present the OCB (dashed black line) of the first case study around the space-ground conjunction time and longitude following Chisham and Freeman [2003, 2004] and Chisham et al. [2004b, 2005a, 2005b, 2005c]. The OCB was nearly along a constant latitude. Figures S3d-f present time series of the spectral width measurements along beams 4, 7, and 10, as a function of latitude. The time series plot allows us to determine the speed of the OCB motion and we determined the speed at each individual beam. Figure S3g presents the electric field along the OCB in the frame of the ionosphere (dotted), and in the frame of the OCB (solid). The latter is the reconnection electric field. The reconnection electric field had essentially the same FWHM as the flow slightly poleward of the OCB (difference being less than the radar spatial resolution).

We note that the process of tracking OCB motion can introduce large uncertainties, especially for our events where the OCB moved very slowly (Figure S1). Given the radar spatial ($\sim 0.3^\circ$) and temporal (2 min) resolution, the speed of OCB has an uncertainty of ~ 300 m/s. This results in a signal to noise ratio generally around or even below one, even though we have not yet considered the measurement error associated with spectral widths or the error of using 150 m/s as the OCB threshold in any given event. A similarly poor signal to noise ratio has been found in Chisham et al. [2008]. This would affect the estimate of the electric field and would reduce the confidence of the results. The flow velocity poleward of the OCB is less affected by the OCB uncertainties.

Given that the electric field profiles at the OCB latitude and the flow velocity profile slightly poleward are about the same, that the echoes are more continuous at higher latitudes, and that our approach is consistent with a number of past works cited above, we think that our approach is sufficient to lead to the conclusion.

- (3) The open-closed field line boundary (OCB) in the ionosphere is insufficiently determined: Lines 390-391 state 'The flow crossed the open-closed field line boundary at 77 degrees MLT. . .'. The determination of the OCB location is not clearly outlined anywhere or displayed clearly on the figures. Indeed, the OCB location in figures 2, 4, and 6 is never sufficiently determined (or visually presented) so it is impossible to know what the longitudinal extent of

flows across the boundary is. The boundary is vaguely discussed as being the equatorward edge of the cusp, which is identified in these figures as being co-located with regions of high Doppler spectral width. (In actuality, comparing figures 2c and 2d, the poleward flow at the equatorward edge of the cusp is slower than that within the polar cap, and most likely extends over a wider longitudinal region.) Although the high spectral width regions circled in these figures may very likely be a result of cusp precipitation, they do not necessarily highlight the full extent of the cusp. High spectral width values are observed within the polar cap at all magnetic local times (see the discussions and references in Chisham et al. (2008) [details above], and Chisham et al. (2007) – A decade of the Super Dual Auroral Radar Network (SuperDARN): scientific achievements, new techniques and future directions – *Surv. Geophys.*, 28, 33-109 [specifically sect. 4, pages 60-67]). If Doppler spectral width is being used to estimate the location of the OCB then it is important to determine the spectral width boundary (SWB) location (see references in the same 2 papers). It is also important that spectral width values are only considered from radar beams that are aligned close to the meridional direction (see Chisham et al. (2005) – The accuracy of using the spectral width boundary measured in off-meridional SuperDARN HF radar beams as a proxy for the open-closed field line boundary – *Ann. Geophys.*, 23, 2599-2604).

Response: The references provided by the reviewer are highly relevant and have been included in the text. The OCB is determined as the 150 m/s spectral width boundary [e.g., Baker et al., 1995, 1997; Chisham and Freeman, 2003] as indicated in the text although we did not present the details in our previous manuscript. The details are now displayed in Figures S1 and S3. We also mark this boundary in Figures 2, 4, and 6 as a black dashed line.

We agree with the reviewer that high spectral width can span across a wide range. But here we look for structures embedded in the spectral width because the existence of a localized enhancement indicates enhanced energy input from the magnetosphere over a finite area. This is consistent with our focus on reconnection bursts. The “cusp” feature we refer to follows the dynamic cusp model where the cusp precipitation is driven by reconnection bursts. To avoid confusion with the traditional cusp, we rename it as enhanced soft electron precipitation.

- (4) Quality and clarity of the figures containing the radar data: The radar data plots in figures 2, 4, and 6 are incredibly messy, cluttered, and difficult to interpret, especially panels a and d, where line-of-sight (LOS) velocity and spectral width are displayed across the radar fields-of-view. These figures need to be simplified. Is all the LOS velocity data required in panel a? Are the merged vectors not information enough? Especially given that the LOS data on their own are open to severe misinterpretation. Can a boundary be determined from the spectral width data (see above) rather than highlighting a vague blob of high spectral width? If such a boundary was determined, then over-plotting this boundary on the velocity vector panels would be highly informative.

Response: We thank the reviewer for the suggestion and have simplified panels a and d by deleting isolated LOS backscatters and minimizing the overlap of backscatters. The OCB has also been overlaid on panels a, b, and c. We mentioned about determination of spectral width boundary. The red blobs in Figures 2d, 4d, and 6d highlight structures of high spectral width which are not related to the OCB determination but enhanced soft electron precipitation.

Reviewer #3

This manuscript uses a combination of satellite and ground-based radar data to estimate the spatial extent of magnetopause reconnection for 3 example events. The motivation for the study is very good and the results are potentially interesting and important but, in my view, the crucial radar analysis falls short of the state of the art and needs improving to support the interpretation. Even if this does not radically change the main results, it would put the results on a sounder footing, better evaluate sources and sizes of uncertainties, and allow the results given here to be compared more objectively to past and future studies. For this reason, I would not recommend publication in its present form. My recommendations are as follows:

1. Follow the state of the art

In the current analysis, evidence for the reconnection X-line is essentially based on looking for high-speed flows in the vicinity of a high radar spectral width region (e.g., Figure 2a-d) and the X-line extent is estimated from a longitudinal profile of northward velocity at a relatively arbitrary magnetic latitude. In my view this is a rather crude analysis and it should be possible to do this better by estimating the profile of the reconnection electric field itself along the open-closed field line boundary (OCB) and its time evolution following the methodology set out in detail in: Chisham, G., et al. (2008), Remote sensing of the spatial and temporal structure of magnetopause and magnetotail reconnection from the ionosphere, *Rev. Geophys.*, 46, RG1004, doi:10.1029/2007RG000223.

Freeman, M. P., G. Chisham, and I. J. Coleman (2007), Remote sensing of reconnection, in *Reconnection of Magnetic Fields*, edited by J. Birn and E. Priest, chap. 4.6, pp. 217–228, Cambridge Univ. Press, New York.

In essence, this method requires the following steps:

a. Identify the OCB objectively at as many locations as possible using available datasets and interpolate in space and time where necessary using suitable models, e.g., figures 6, 8, 9, 11 in Chisham et al (2008).

b. Estimate the reconnection electric field along the OCB by measuring the electric field component parallel to the boundary (or $E \times B$ velocity component perpendicular to it) in the rest frame of the generally moving boundary, e.g., figure 13 in Chisham et al. (2008).

c. Plot profiles of the reconnection electric field versus MLT over the time interval of interest. Use the zero crossing locations of these profiles to estimate the MLT extent of reconnection as a function of time, e.g., figure 7 of Pinnock et al., (2003), The location and rate of dayside reconnection during an interval of southward interplanetary magnetic field, *Ann. Geophys.*, 21, 1467–1482.

d. Project the MLT extent to the magnetopause using a suitable model to estimate the X-line length and its evolution and to compare with in-situ spacecraft observations of presence or absence of reconnection, e.g., figure 8 of Pinnock et al. (2003).

The authors' analysis is only a very crude approximation to this. Particular areas of improvement that I would recommend include:

Response: We thank the reviewer for the detailed comments and instructions. We realize that our view of “X-line” is different from the reviewer's and this seems to have affected the understanding of how an X-line extent should be measured. In our original terminology we used “magnetic separator” to refer to the global configuration along which reconnection occurs at various rates, and used “X-lines” to refer to regions of strong reconnection, i.e., reconnection bursts, which could activate over a segment of the magnetic separator. The focus of the paper is the latter, as motivated by progresses in recent numerical simulations [Shay et al., 2003; Sheperd and Cassak, 2012]. To avoid confusion, we replace “extent of X-lines” with “extent of reconnection bursts”.

The references of X-line extent given by the reviewer provide valuable groundwork of clarifying the scope of this study. We rewrote the first paragraph as

“...Reconnection tends to occur at sites of strictly anti-parallel magnetic fields as anti-parallel reconnection [e.g. Crooker, 1979; Luhmann et al., 1984], or occur along a line passing through the subsolar region as component reconnection [e.g. Sonnerup, 1974; Gonzalez and Mozer, 1974]. Evidence shows either or both can occur at the magnetopause and the overall reconnection extent can span from a few up to 40 Re [*Paschmann et al.*, 1986; *Gosling et al.*, 1990; *Phan and Paschmann*, 1996; *Coleman et al.*, 2001; *Phan et al.*, 2001, 2003; *Chisham et al.*, 2002, 2004, 2008; *Petrinec and Fuselier*, 2003; *Fuselier et al.*, 2002, 2003, 2005, 2010; *Petrinec and Fuselier*, 2003; *Pinnock et al.*, 2003; *Bobra et al.*, 2004; *Trattner et al.*, 2004, 2007, 2008, 2017; *Trenchi et al.*, 2008]. However, reconnection does not occur uniformly across this configuration but has spatial variations [*Pinnock et al.*, 2003; *Chisham et al.*, 2008]. The local time extent of reconnection bursts is the focus of this study.”

The methodology adopted by our paper has been commonly used for studying reconnection bursts. It is a common approach to measure the flow extent at a latitude poleward of the OCB as the reconnection extent [*Goertz et al.*, 1985; *Pinnock et al.*, 1993, 1995; *Provan and Yeoman*, 1999; *Thorolfsson et al.*, 2000; *McWilliams et al.*, 2001a, 2001b; *Elphic et al.*, 1990; *Denig et al.*, 1993; *Neudegg et al.*, 1999, 2000; *Lockwood et al.*, 2001; *Wild et al.*, 2001, 2003, 2007; *McWilliams et al.*, 2004; *Zhang et al.*, 2008]. Based on the snapshots the flow extent did not change much over a 2-3° displacement in latitude. Considering these numerous past works, methodology has followed a standard approach.

However, we appreciate the reviewer’s suggestion and think that it is a good idea to compare our flow velocity profile with the reconnection electric field profile derived following Pinnock et al. [2003], Freeman et al. [2007], Chisham et al. [2008]. We have followed the helpful instructions given by the reviewer and presented our result in Figure S3 based on event #1 (replaced with a new event following the advice of reviewer #1). Details can be found below.

2. Improved estimates of the OCB (step 1a above)

a. The authors use a 150 m/s spectral width threshold to estimate the OCB but then apply it rather vaguely by drawing a red contour in figures 2d, 4d, 6d which doesn’t match the 150 m/s threshold everywhere. The authors then largely ignore this anyway by using examining the ExB velocity on a fixed latitude circle that is generally poleward of where they say the OCB is. For example, for the first event in section 3.1.2, in lines 293-295 it is said that the OCB is at 77 deg latitude based on the spectral width in figure 2d but in lines 360-366 the 80 deg latitude circle is used as the OCB for the velocity cross-section shown in figure 2f. Similarly, in section 3.2.2, it is 77 deg latitude (lines 390-391) from figure 4d and 79 deg latitude (figure 4 caption) used for figure 4f. And in section 3.2.2, it is 80 deg latitude (figure 6 caption) used for figure 6g,h but the spectral width boundary is unstated and appears to be at lower latitude (at about the projected THA position).

b. According to the following references it should be possible to estimate the OCB from spectral widths at a wide range of local times using the method of Chisham and Freeman (2004) and I recommend that this be attempted more carefully and objectively.

Chisham, G., and M. P. Freeman (2003), A technique for accurately determining the cusp-region polar cap boundary using SuperDARN HF radar measurements, *Ann. Geophys.*, 21, 983–996.

Chisham, G., and M. P. Freeman (2004), An investigation of latitudinal transitions in the SuperDARN Doppler spectral width parameter at different magnetic local times, *Ann. Geophys.*, 22, 1187–1202.

Chisham, G., M. P. Freeman, and T. Sotirelis (2004a), A statistical comparison of SuperDARN spectral width boundaries and DMSPP particle precipitation boundaries in the nightside ionosphere, *Geophys. Res. Lett.*, 31, L02804, doi:10.1029/2003GL019074.

Chisham, G., M. P. Freeman, T. Sotirelis, R. A. Greenwald, M. Lester, and J.-P. Villain (2005a), A statistical comparison of SuperDARN spectral width boundaries and DMSP particle precipitation boundaries in the morning sector ionosphere, *Ann. Geophys.*, 23, 733–743.

Chisham, G., M. P. Freeman, T. Sotirelis, and R. A. Greenwald (2005b), The accuracy of using the spectral width boundary measured in off-meridional SuperDARN HF radar beams as a proxy for the open-closed field line boundary, *Ann. Geophys.*, 23, 2599–2604.

Chisham, G., M. P. Freeman, M. M. Lam, G. A. Abel, T. Sotirelis, R. A. Greenwald, and M. Lester (2005c), A statistical comparison of SuperDARN spectral width boundaries and DMSP particle precipitation boundaries in the afternoon sector ionosphere, *Ann. Geophys.*, 23, 3645–3654.

c. The OCB can also be estimated from other data, such as DMSP particle precipitation. It seems that this data might be available for the events studied, see <https://heliophysicsdata.sci.gsfc.nasa.gov/websearch/dispatcher> Even if not particularly close in MLT or UT it may be useful as a constraint.

d. The T89 model projections of the THA magnetopause crossing to the ionosphere in Figures 4 and 6 appear to agree with the OCB location estimated from the spectral width. It would thus seem reasonable to use the model to estimate the OCB location in the ionosphere at all dayside MLT at this UT.

The projected location of THE may be different in these two cases because from Figure 3 there is evidently a rapid outward expansion of the magnetopause from 9.4 RE to 10.2 RE between 1826 and 1828 UT which would need appropriate re-scaling of the model to capture, and in Figure 5 the spacecraft are separated by over 30 min in time and so again the model conditions are probably different. In these cases, and for the figure 2 event, it seems reasonable to explore simple scalings of the T89 model that would fit the magnetopause crossing location of each spacecraft and see if this improves the projected location of the spacecraft with respect to the spectral width boundary. If so, then the model could be used to extrapolate to all dayside MLT.

e. Alternatively, a simple offset circle model is commonly a good approximation to the OCB, whose free parameters could be constrained by spectral width and possibly DMSP data. This would at least be an improvement on assuming a latitudinal circle that is rather unrelated to the spectral width boundary.

In all of the above cases, limitations and assumptions can be assessed by error and sensitivity analyses. For example, how are the results 1b-d above affected by changing the inferred boundary by 1 degree say?

Response: Figures S3a-c present the OCB of event #1 around the space-ground conjunction time and longitude. We have identified the OCB more precisely following Chisham and Freeman [2003, 2004] and Chisham et al. [2004, 2005a, 2005b, 2005c] and it is drawn as the dashed black line. The OCB in this event was found nearly along a constant latitude. THEMIS satellite footprints were mapped very closely to the OCB.

3. Take account of the generally moving OCB (step 1b above)

As emphasised in the references in 1 above, the reconnection rate is the electric field in the frame of the moving OCB and this can sometimes affect the inference of whether reconnection is occurring or not, e.g., see Figure 13 of Chisham et al. (2008). Some account of this should be taken in the present analysis as it may affect the edges of the inferred reconnection region in particular and hence the FWHM.

Response: Figures S3d-f present time series of the spectral width measurements along beams 4, 7, and 10, as a function of latitude. The time series plot allows us to determine the speed of the OCB motion and we determined the speed at each individual beam. Note that the OCB motion was longitudinally dependent and was faster around eastern than western beams.

4. Project the ExB velocity perpendicular to the boundary (relevant to step 1c above)

Given the strong rotation of the flow seen in figure 2 in particular, consideration should be given of the effect of uncertainties in the assumed orientation of the OCB on the projected flow component across it as this could change the inferred X-line extent.

Response: Figure S3g presents the electric field along the OCB in the frame of the ionosphere (dotted), and in the frame of the OCB (solid). The latter is the reconnection electric field. The reconnection electric field had essentially the same FWHM as the flow slightly poleward of the OCB (difference being less than the radar spatial resolution).

Although the method suggested by the reviewer has its advantage, we note that the process of tracking OCB motion can introduce large uncertainties, especially for our events where the OCB moved very slowly (Figure S1). Given the radar spatial ($\sim 0.3^\circ$) and temporal (2 min) resolution, the speed of OCB has an uncertainty of ~ 300 m/s. This results in a signal to noise ratio generally around or even below 1 for the OCB speed, even though we have not yet considered the measurement error associated with spectral widths or the error of using 150 m/s as the OCB threshold in any given event. A similarly poor signal to noise ratio has been found in Chisham et al. [2008]. This would affect the estimate of the electric field and would reduce the confidence of the results. Therefore it is not entirely clear to us whether deriving the reconnection electric field serves as a better methodology for the purpose of our study.

Our study does not discuss the magnitude of the reconnection electric field, but the width is the focus. The flow velocity poleward of the OCB is less affected by the OCB uncertainties. Given that the electric field profiles at the OCB latitude and the flow velocity profile slightly poleward are about the same, that the echoes are more continuous at higher latitudes, and that our approach is consistent with a number of past works cited above, we think that our approach is sufficient to lead to the conclusion.

The above discussion has been clarified in the text as

“It is noteworthy mentioning that the velocity profile obtained above approximates to the profile of reconnection electric field along the open-closed field line boundary (details in Figure S3). Reconnection electric field can be estimated by measuring the flow across the open-closed field line boundary in the reference frame of the boundary [Pinnock et al., 2003; Freeman et al., 2007; Chisham et al., 2008]. However, a precise determination of the boundary motion is subject to radar spatial and temporal resolution and for a slow motion like events studied in this paper (Figure S1), the signal to noise ratio is lower than one. For this reason this paper focuses on the velocity profile poleward of the open-closed field line boundary, which is less affected by the error associated with the boundary.”

We did not consider the OCB location beyond the radar FOV because this study is about flows in the satellite-ground conjunction region (not the entire X-line extent). Since the flow FWHM is confined in the radar FOV, our conclusion does not rely on flow or OCB outside the radar FOV.

5. Improved consideration of the temporal evolution

The current analyses are strongly biased towards comparisons of magnetopause and ionospheric observations of reconnection at a common instant. Given the uncertainties in how reconnection may evolve at the magnetopause, and the ionospheric response times, it would be helpful to repeat the analysis shown in figure 2f, 4f, and 6g,h at some sampling frequency throughout the intervals shown in figures 2e, 4e, and 6e,f. The temporal evolution of los data shown in figures 2e, 4e, and 6e,f are a rather poor proxy by which to estimate the evolution of X-line extent and something similar to figure 7 of Pinnock

et al (2003) would be very interesting to see, especially for the inferred complex evolution of the Apr 29 event.

Response: As clarified above, we target reconnection bursts whose extent is by convention measured as the ionospheric flow width. We also focus on the times of satellite magnetopause crossings in order to achieve a space-ground comparison.

6. Discrepancies in magnetopause to ionosphere projection (step 1d above)

The magnetopause crossings of spacecraft THA and THD in figure 2, and THE in figure 4 (and possibly figure 6 too) project several degrees of latitude away from the expected OCB location based on spectral width. This suggests that the estimation of X-line extent at the magnetopause from that inferred in the ionosphere will be in error because it is based on the same T89 model that seemingly incorrectly projects the satellite position to the ionosphere. As mentioned in 2d above, it would be helpful to try to estimate the uncertainty by considering whether there is some simple rescaling of the T89 model that would reduce the discrepancy in the magnetopause-to-ionosphere projection.

I would also add that the description of the mapping method given in lines 372-376 is too vague to allow others to reproduce your method. It also seems that you use the same T89 mapping factor of 55 for all three events, which seems questionable, e.g., solar wind dynamic pressure is 50% larger for Apr 19 event. It also implies that the factor is the same for all MLT which is unlikely I think, especially over the 10 Re magnetopause extent inferred for the Apr 29 event. Please could you improve your method description and assess the associated uncertainties.

Response: We would like to clarify that the T89 model is Kp based and does not have solar wind input. Our events all occurred around Kp=2 and that's why the mapping factor is similar.

In the new Figure 2 (see attachment), the satellite footprints were mapped within the radar FOV and nearly aligned with the OCB. In the Figure 4 event, the 'outward magnetopause motion' does not appear to be due to IMF or solar wind pressure pulses because neither changed substantially. Local distortions of the magnetopause may be a possibility. In any case, there is no known reliable way to modify the model and thus we choose to take the best estimate from the model. In the Figure 6 case, THE crossed the magnetopause later than THA, and at the time of Figure 6 THE was still inside the magnetosphere. THE footprint later on moved to the OCB as the satellite crossed the magnetopause.

As mentioned above, our study does not concern OCB outside the radar FOV. Although we agree that the OCB could be obtained by model magnetopause mapping or addition of DMSP, it does not affect the reconnection burst extent within the radar FOV.

7. I would recommend that you reference and discuss the following first 5 papers in lines 136-141 as these have done a similar comparison of simultaneous reconnection evidence from space and ground to infer X-line length. I would also recommend that you consider the implications of these and the sixth reference to your discussion in section 3.4 as they seem to be relevant to the factors affecting X-line extent (e.g., IMF orientation, component or anti-parallel reconnection, turbulence):

Phan, T.D., Freeman, M.P., Kistler, L.M. et al. *Earth Planet Sp* (2001) 53: 619. <https://doi.org/10.1186/BF03353281>

Pinnock, M., G. Chisham, I. J. Coleman, M. P. Freeman, M. Hairston, and J.-P. Villain (2003), The location and rate of dayside reconnection during an interval of southward interplanetary magnetic field, *Ann. Geophys.*, 21, 1467–1482.

Coleman, I. J., G. Chisham, M. Pinnock, and M. P. Freeman (2001), An ionospheric convection signature of antiparallel reconnection, *J. Geophys. Res.*, 106, 28,995–29,007.

Chisham, G., I. J. Coleman, M. P. Freeman, M. Pinnock, and M. Lester (2002), Ionospheric signatures of split reconnection X-lines during conditions of IMF $B_z < 0$ and $|B_y|/|B_z|$: Evidence for the antiparallel merging hypothesis, *J. Geophys. Res.*, 107(A10), 1323, doi:10.1029/2001JA009124.

Chisham, G., M. P. Freeman, I. J. Coleman, M. Pinnock, M. R. Hairston, M. Lester, and G. Sofko (2004b), Measuring the dayside reconnection rate during an interval of due northward interplanetary magnetic field, *Ann. Geophys.*, 22, 4243–4258

Coleman, I. J., and M. P. Freeman (2005), Fractal reconnection structures on the magnetopause, *Geophys. Res. Lett.*, 32, L03115, doi:10.1029/2004GL021779.

Response: We modify the text in Section 3.4 as

“...The IMF B_x and B_y components are known to modify the magnetic shear across the magnetopause and to affect the occurrence location of reconnection. Studies have found that small $|B_y|/|B_z|$ relates to anti-parallel and large $|B_y|/|B_z|$ to component reconnection [Coleman *et al.*, 2001; Chisham *et al.*, 2002; Trattner *et al.*, 2007]. Large $|B_x|/|B|$, i.e. cone angle, also favors formation of high-speed magnetosheath jets [Archer and Horbury, 2013; Plaschke *et al.*, 2013] of a few R_e in scale size, resulting in a turbulent magnetosheath environment for reconnection to occur [Coleman, and Freeman, 2005]”

24 Local time extent of magnetopause reconnection ~~X~~-linesbursts using space-ground coordination

25

26 Ying Zou^{1,2}, Brian M. Walsh³, Yukitoshi Nishimura^{4,5}, Vassilis Angelopoulos⁶, J.
27 Michael Ruohoniemi⁷, Kathryn A. McWilliams⁸, Nozomu Nishitani⁹

28

29 1. Department of Astronomy and Center for Space Physics, Boston University, Massachusetts,
30 USA

31 2. Cooperative Programs for the Advancement of Earth System Science, University Corporation
32 for Atmospheric Research, Boulder, Colorado, USA

33 3. Department of Mechanical Engineering and Center for Space Physics, Boston University,
34 Boston, Massachusetts, USA

35 4. Department of Electrical and Computer Engineering and Center for Space Sciences, Boston
36 University, Boston, Massachusetts, USA

37 5. Department of Atmospheric and Oceanic Sciences, University of California, Los Angeles,
38 California, USA

39 6. Department of Earth, Planetary and Space Sciences, University of California, Los Angeles,
40 California, USA

41 7. The Bradley Department of Electrical and Computer Engineering, Virginia Tech, Blacksburg,
42 Virginia, USA

43 8. Institute of Space and Atmospheric Studies, University of Saskatchewan, Saskatoon,
44 Saskatchewan, Canada

45 9. Center for International Collaborative Research, Institute for Space-Earth Environmental
46 Research, Nagoya University, Nagoya, Japan

70 Corresponding author: Ying Zou

71 1. Department of Astronomy and Center for Space Physics, Boston University, Massachusetts,

72 USA

73 2. Cooperative Programs for the Advancement of Earth System Science, University Corporation

74 for Atmospheric Research, Boulder, Colorado, USA

75 yingzou@bu.edu

76

77 Keyword: 2784 Solar wind–magnetosphere interactions; 2724 Magnetopause, cusp, and

78 boundary layers; 7835 Magnetic reconnection

79

80

81

82

83

84

85

86

87

88

89

90

91

92

Formatted

93 Abstract

94 Magnetic reconnection ~~bursts~~X-lines can vary considerably in ~~spatial extents~~length. At the
95 Earth's magnetopause, the ~~length~~extent generally corresponds to the extent in local time. The
96 extent has been probed by multi-spacecraft crossing the magnetopause, but the estimates have
97 large uncertainties because of the assumption of spatially continuous reconnection activity a
98 ~~continuous X-line~~ between spacecraft and the lack of information beyond areas of spacecraft
99 coverage. The limitations can be overcome by using ~~The extent has also been inferred by~~ radars
100 examining as fast ionospheric flows moving anti-sunward across the open-closed field line
101 boundary, ~~but whether a particular ionospheric flow results from reconnection needs to be~~
102 ~~confirmed.~~ We therefore infer the ~~To achieve a reliable interpretation, we compare X-line~~ extents
103 of reconnection bursts using coordinated observations of ~~probed by~~ multi-spacecraft and radars for
104 three conjunction events. We find that when reconnection is active at only one spacecraft, only the
105 ionosphere conjugate to this spacecraft shows a channel of fast anti-sunward flow. When
106 reconnection is active at two spacecraft and the spacecraft are separated by $<1 R_e$, the ionosphere
107 conjugate to both spacecraft shows a channel of fast anti-sunward flow. The consistency allows us
108 to determine the ~~X-line~~reconnection burst extent by measuring the ionospheric flows. The flow
109 extent is ~~520~~260, 572, and 1260 km, corresponding to ~~an X-line~~reconnection burst extent of ~~4~~3, 5,
110 and 11 R_e . This strongly indicates that both spatially patchy (a few R_e) and spatially continuous
111 and extended reconnection ($>10 R_e$) are possible forms of reconnection at the magnetopause.
112 Interestingly, the extended reconnection develops from a localized patch via spreading across local
113 time. Potential effects of IMF B_x and B_y on the ~~X-line~~reconnection burst extent are discussed.

114

115

139
140
141
142
143
144
145
146
147
148
149
150
151
152
153
154
155
156
157
158
159
160
161

1. Introduction

A long-standing question in magnetic reconnection is what is the spatial extent of reconnection in the direction normal to the reconnection plane. At the Earth's magnetopause, for a purely southward IMF, this corresponds to the extent in the local time or azimuthal direction. The extent of reconnection has significant relevance to solar wind-magnetosphere coupling, as it controls the amount of energy being passed through the boundary from the solar wind into the magnetosphere and ionosphere. Magnetopause reconnection tends to occur at sites of strictly anti-parallel magnetic fields as anti-parallel reconnection [e.g. Crooker, 1979; Luhmann et al., 1984], or occur along a line passing through the subsolar region as component reconnection [e.g. Sonnerup, 1974; Gonzalez and Mozer, 1974]. Evidence shows either or both can occur at the magnetopause, and the overall reconnection extent can span from a few to 40 Re [Paschmann et al., 1986; Gosling et al., 1990; Phan and Paschmann, 1996; Coleman et al., 2001; Phan et al., 2001, 2003; Chisham et al., 2002, 2004, 2008; Petrinec and Fuselier, 2003; Fuselier et al., 2002, 2003, 2005, 2010; Petrinec and Fuselier, 2003; Pinnock et al., 2003; Bobra et al., 2004; Trattner et al., 2004, 2007, 2008, 2017; Trenchi et al., 2008]. However, reconnection does not occur uniformly across this configuration but has spatial variations [Pinnock et al., 2003; Chisham et al., 2008]. The local time extent of reconnection bursts is the focus of this study. This, however, does not represent the extent of active reconnection X lines, as reconnection may not be active at all portions of this configuration, but can occur at discontinuous patches or over a limited segment only.

Formatt
Formatt
Formatt
Formatt

185 Numerical models show that reconnection bursts tends to occur at magnetic separators, i.e. at
186 the junction between regions of different magnetic field topologies, and global MHD models have
187 identified a spatially continuous separator along the magnetopause [Dorelli *et al.*, 2007; Laitinen
188 *et al.*, 2006, 2007; Haynes and Parnell, 2010; Komar *et al.*, 2013; Glozer *et al.*, 2016]. However,
189 little is known about where and over what range along the separators reconnection is active.
190 Reconnection in numerical simulations can be activated by introducing perturbations of the
191 magnetic field or can grow spontaneously with instability or resistivity inherent in the system [e.g.
192 Hesse *et al.*, 2001; Scholer *et al.*, 2003]. When reconnection develops as patches (as due to the
193 instabilities or localized perturbations), the patches can spread in the direction out of the
194 reconnection plane [Huba and Rudakov, 2002; Shay *et al.* 2003; Lapenta *et al.*, 2006; Nakamura
195 *et al.*, 2012; Shepherd and Cassak, 2012; Jain *et al.*, 2013]. The patches either remain patchy after
196 spreading if the current layer is thick, or form an extended X-line if the current layer is already
197 thin [Shay *et al.*, 2003].

198 Studies have attempted to constrain the extent of reconnection bursts ~~The extent of reconnection~~
199 ~~X-lines has been observationally determined~~ based on fortuitous satellite conjunctions where the
200 satellites detect signatures of active reconnection at the magnetopause at different local times
201 nearly simultaneously [Phan *et al.*, 2000, 2006; Walsh *et al.*, 2014a, 2014b, 2017]. The satellites
202 were separated by a few R_e in Phan *et al.* [2000] and Walsh *et al.* [2014a, 2014b, 2017], and >10
203 R_e in Phan *et al.* [2006], and this is interpreted as the ~~X-line~~ reconnection being ~~longer wider~~
204 a few R_e and even $10 R_e$, respectively. At the magnetopause, ~~X-lines~~ reconnection bursts of a few
205 R_e are often referred to as spatially patchy [e.g., Fear *et al.*, 2008, 2010], and ~~X-lines~~ reconnection
206 bursts of $>10 R_e$ are spatially extended [Dunlop *et al.*, 2011; Hasegawa *et al.*, 2016]. The term
207 patchy has also been used to describe the temporal characteristics of reconnection [e.g. Newell and

Formatted

208 Meng, 1991]. But this paper primarily focuses on the spatial properties. The extent of ~~X-~~
209 linesreconnection bursts has been alternatively determined by studying the structures of newly
210 reconnected flux tubes, i.e., flux transfer events (FTEs) [*Russell and Elphic, 1978; Haerendel et*
211 *al., 1978*]. Conceptual models regard FTEs either as azimuthally narrow flux tubes that intersect
212 the magnetopause through nearly circular holes, as formed by spatially patchy ~~X-linesreconnection~~
213 [*Russell and Elphic, 1978*], or as azimuthally elongated bulge structures or flux ropes that extend
214 along the magnetopause, as formed by spatially extended ~~X-linesreconnection~~ [*Scholer, 1988;*
215 *Southwood et al., 1987; Lee and Fu, 1985*]. FTEs have been observed to be $>$ or <2 R_E wide in
216 local time [*Fear et al., 2008, 2010; Wang et al., 2005, 2007*]. FTEs have even been observed across
217 $\sim 20 R_E$ from the subsolar region to the flanks [*Dunlop et al., 2011*]. But it is unclear whether these
218 FTEs are branches of one extended bulge or flux rope, or multiple narrow tubes formed
219 simultaneously. When the satellites are widely spaced, it is in general questionable whether an ~~X-~~
220 line reconnection burst/FTE is spatially continuous between the satellites or whether satellites
221 detect the same moving ~~X-linereconnection burst~~/FTE. Satellites with a small separation may
222 possibly measure the same ~~X-linereconnection burst~~/FTE, but only provide a lower limit estimate
223 of the extent. An ~~X-line~~ reconnection burst/FTE may also propagate or spread between satellite
224 detection but satellite measurements cannot differentiate the spatial and temporal effects.

225 This situation can be improved by studying ionospheric signatures of reconnection bursts and
226 FTEs, since their spatial sizes in the ionosphere can be obtained from wide field ground
227 instruments or Low-Earth orbit spacecraft. The ionospheric signatures include poleward moving
228 auroral forms (PMAFs), channels of fast flows moving anti-sunward across the open-closed field
229 line boundary [e.g., *Southwood, 1985*], and cusp precipitation [*Lockwood and Smith, 1989, 1994;*
230 *Smith et al., 1992*]. Radar studies have shown that the flows can differ considerably in size, varying

231 from tens of km [Oksavik et al., 2004, 2005], to hundreds of km [Goertz et al., 1985; Pinnock et
232 al., 1993, 1995; Provan and Yeoman, 1999; Thorolfsson et al., 2000; McWilliams et al., 2001a,
233 2001b], and to thousands of km [Provan et al., 1998; Nishitani et al., 1999; Provan and Yeoman,
234 1999]. A similarly broad distribution has been found for PMAFs [e.g. Sandholt et al., 1986, 1990;
235 Lockwood et al., 1989, 1990; Milan et al., 2000, 2016] and the cusp [Crooker et al., 1991; Newell
236 and Meng, 1994; Newell et al., 2007]. This range of spatial sizes in the ionosphere approximately
237 corresponds to a range from <1 to >10 Re at the magnetopause. However, care needs to be taken
238 when interpreting the above ionospheric features, since they could also form due to other drivings
239 such as solar wind dynamic pressure pulses [Lui and Sibeck, 1991; Sandholt et al., 1994]. An
240 unambiguous proof of their connection to magnetopause reconnection requires simultaneous
241 space-ground coordination [Elphic et al., 1990; Denig et al., 1993; Neudegg et al., 1999, 2000;
242 Lockwood et al., 2001; Wild et al., 2001, 2005, 2007; McWilliams et al., 2004; Zhang et al., 2008].

243 Therefore a reliable interpretation of reconnection ~~burst X-line~~ extent has been difficult due to
244 observation limitations. We will address this by comparing ~~X-line~~the extents probed by multi-
245 spacecraft and radars using space-ground coordination. On one hand, this enables us to investigate
246 whether ~~X-lines are~~reconnection spans continuously between satellites, and how wide
247 reconnection~~X-lines~~ extends beyond satellites. On the other hand, this helps to determine whether
248 reconnection is the driver of ionospheric disturbances and whether the in-situ extent is consistent
249 with the ionospheric disturbance extent.

250 It may be noteworthy to point out that we only address the ~~X-line~~reconnection extent in the local
251 time direction, similarly to previous observations. If the reconnection X-line has a tilted orientation
252 relative to the equatorial plane, the local time extent will be shorter than the total extent. How X-
253 lines tilt is a subject of ongoing research. Various models have been proposed to predict the tilt

277 [Alexeev et al., 1998; Moore et al., 2002; Trattner et al., 2007; Swisdak and Drake, 2007;
278 Borovsky, 2013; Hesse et al., 2013] but their performance is still under test [e.g., Komar et al.,
279 2015]. The local time extent is what determines the amount of magnetic flux opened in the solar
280 wind-magnetosphere coupling [e.g. Newell et al., 2007].

281

282 2. Methodology

283 We use conjugate measurements between the Time History of Events and Macroscale
284 Interactions during Substorms (THEMIS) [Angelopoulos, 2008] and Super Dual Auroral Network
285 (SuperDARN) [Greenwald et al., 1995]. We focus on intervals when the IMF in OMNI data
286 remains steadily southward. We require that two of the THEMIS satellites fully cross the
287 magnetopause nearly simultaneously and that the satellite data provide clear evidence for
288 reconnection occurring or not. The full crossings are identified by a reversal of the Bz magnetic
289 field and a change in the ion energy spectra. The requirements of nearly simultaneous crossings
290 and steady IMF conditions help to reduce the spatial-temporal ambiguity by satellite measurements,
291 where the presence/absence of reconnection signatures at different local times likely reflects
292 spatial structures of reconnection. Reconnection can still possibly vary between the two satellite
293 crossings, and we use the radar measurements to examine whether the reconnection ~~X-line~~ of
294 interest has continued to exist and maintained its spatial size.

295 Fluid (MHD) evidence of magnetopause reconnection includes plasma bulk flow acceleration
296 at the magnetopause. This acceleration should be consistent with the prediction of tangential stress
297 balance across a rotational discontinuity, i.e. Walen relation [Hudson, 1970; Paschmann et al.,
298 1979]. The Walen relation is expressed as

299
$$\Delta V_{predicted} = \pm(1 - \alpha_1)^{1/2}(\mu_0 \rho_1)^{-1/2}[B_2(1 - \alpha_2)/(1 - \alpha_1) - B_1] \quad (1)$$

323 Where ΔV is the change in the plasma bulk velocity vector across the discontinuity. B and ρ are
324 the magnetic field vector and plasma mass density. μ_0 is the vacuum permeability. $\alpha = (p_{\parallel} - p_{\perp})\mu_0/B^2$
325 is the anisotropy factor where p_{\parallel} and p_{\perp} are the plasma pressures parallel and perpendicular
326 to the magnetic field. The magnetic field and plasma moments are obtained from the fluxgate
327 magnetometer (FGM) [Auster *et al.*, 2008] and the ElectroStatic Analyzers (ESA) instrument
328 [McFadden *et al.*, 2008]. The plasma mass density is determined using the ion number density,
329 assuming a mixture of 95% protons and 5% helium. The subscripts 1 and 2 refer to the reference
330 interval in the magnetosheath and to a point within the magnetopause, respectively. The
331 magnetosheath reference interval is a 10-s time period just outside the magnetopause. The point
332 within the magnetopause is taken at the maximum ion velocity change across the magnetopause.
333 We ensure that the plasma density at this point is >20% of the magnetosheath density to avoid the
334 slow-mode expansion fan [Phan *et al.*, 1996]. We compare the observed ion velocity change with
335 the prediction from the Walen relation. The level of agreement is measured by $\Delta V^* =$
336 $\Delta V_{obs} \cdot \Delta V_{predicted} / |\Delta V_{predicted}|^2$, following Paschmann *et al.* [1986]. Here ΔV_{obs} is the
337 observed ion velocity change.

338 A kinetic signature of reconnection is found as D-shaped ion distributions at the magnetopause.
339 As magnetosheath ions encounter newly opened magnetic field lines at the magnetopause, they
340 either transmit through the magnetopause entering the magnetosphere or reflect at the boundary.
341 The transmitted ions have a cutoff parallel velocity (i.e. de-Hoffman Teller velocity) below which
342 no ions could enter the magnetosphere. The D-shaped ion distributions are deformed into a
343 crescent shape as ions travel away from the reconnection site [Broll *et al.* 2017]~~persist from the~~
344 ~~active reconnection region at the magnetopause into the ionosphere where they appear as cusp ion~~
345 ~~steps~~are [McWilliams *et al.*, 2004]. We require the satellites to operate in the Fast Survey or Burst

346 mode in which ion distributions are available at 3 s resolution.

347 We determine reconnection being active if the plasma velocity change across the magnetopause
348 is consistent with the Walen relation with $\Delta V^* \geq 0.5$, and if the ions at the magnetopause show a
349 D shape distribution. Reconnection is deemed absent if neither of the two signatures is detected.
350 We require that at least one of the two satellites observe reconnection signatures. Reconnection is
351 regarded as ambiguous if only one of the two signatures is detected, and such reconnection is
352 excluded from our analysis.

353 We mainly use the three SuperDARN radars located at Rankin Inlet (RKN, geomagnetic 72.6°
354 MLAT, -26.4° MLON), Inuvik (INV, 71.5° MLAT, -85.1° MLON), and Clyde River (CLY, 78.8°
355 MLAT, 18.1° MLON) to measure the ionospheric convection near the dayside cusp. The three
356 radars have overlapping field of views (FOVs), enabling a reliable determination of the 2-d
357 convection velocity. The FOVs cover the ionosphere $>75^\circ$ MLAT, covering the typical location
358 of the cusp under weak and modest solar wind driving conditions [i.e., *Newell et al.*, 1989] and the
359 high occurrence region of pulsed ionospheric flows [*Provan and Yeoman*, 1999] with high spatial
360 resolution. Data from Saskatoon (SAS, 60° MLAT, -43.8° MLON) and Prince George (PGR, 59.6°
361 MLAT, -64.3° MLON) radars are also used when data are available. The measurements of these
362 two radars at far range gates can overlap with the cusp. The radar data have a time resolution of 1-
363 2 min. We focus on observations ± 3 h MLT from magnetic noon (approximately 1600-2200 UT).
364 The satellite footprints should be mapped close to the radar FOVs under the Tsyganenko (T89)
365 model [*Tsyganenko*, 1989]. Footprints mapped using different Tsyganenko (e.g., T96 or T01
366 [*Tsyganenko*, 1995, 2002a, 2002b]) models have similar longitudinal locations (difference <100
367 km), implying the longitudinal uncertainty of mapping to be small. The latitudinal uncertainty can
368 be inferred by referring to the open-closed field line boundary as estimated using the 150 m/s

369 spectral width boundary [e.g., *Baker et al.*, 1995, 1997; *Chisham and Freeman*, 2003]. And T89
370 has given the smallest latitudinal uncertainty for the studied events. We surveyed years 2014-2016
371 during the months when the satellite apogee was on the dayside, and found 6 such conjunctions.

372 The ionospheric signature of reconnection burst includes fast anti-sunward flows moving across
373 the open-closed field line boundary. We obtain the flow velocity vectors by merging line-of-sight
374 (LOS) measurements at the radar common FOVs [*Ruohoniemi and Baker*, 1998], and these merged
375 vectors reflect the true ionospheric convection velocity. However, the radar common FOVs are
376 hundreds of km wide only, which can be too small to cover the full azimuthal extent of the
377 reconnection-related flows (which are up to thousands of km wide). We therefore also reconstruct
378 the velocity field using the Spherical Elementary Current Systems (SECS) method [*Amm et al.*,
379 2010]. Similar to the works by *Ruohoniemi et al.* [1989] and *Bristow et al.* [2016], the SECS
380 method reconstructs a divergence-free flow pattern using all LOS velocity data. We refer to these
381 velocities as SECS velocities. The accuracy of SECS velocities can be validated by comparing to
382 the LOS measurements and the merged vectors. SECS velocities work best in regions with dense
383 echo coverage and those around sparse echoes are not reliable and thus are excluded from our
384 analysis.

385 The third way of obtaining a velocity field is Spherical Harmonic Fit (SHF). This method uses
386 the LOS measurements and a statistical convection model to fit the distribution of electrostatic
387 potential, which is expressed as a sum of spherical harmonic functions [*Ruohoniemi and Baker*,
388 1998]. The statistical model employed here is *Cousins and Shepherd* [2010]. While this method
389 may suppress small or meso-scale velocity details, such as, sharp flow gradients or flow vortices,
390 we compare SHF velocities with the LOS measurements and merged vectors to determine how
391 well the SHF velocities depict the velocity details.

415 Among the six events we identified, we present three representative conjunction events in
416 Sections 3.1-3.3. The time separation of magnetopause crossings by two satellites are 1, 2, and 30
417 min. While the time separation for the third case is somewhat long, we distinguish the spatial and
418 temporal effects using the radar data. Although the three events occurred under similar IMF Bz
419 conditions, the reconnection-related flows in the ionosphere had an azimuthal extent varying from
420 a few hundred km (Sections 3.1-3.2) to more than a thousand km wide (Section 3.3). This
421 corresponds to ~~X-lines~~reconnection bursts of a few to >10 Re ~~widelong~~, indicating that both
422 spatially patchy (a few Re) and spatially continuous and extended reconnection (>10 Re) are
423 possible forms of reconnection at the magnetopause. Interestingly, the extended reconnection was
424 found to arise from a spatially localized patch that spreads azimuthally. Potential effects of IMF
425 Bx and By on the reconnection burst extent are discussed in Section 3.4.

426 Note that reconnection can happen over various spatial and temporal scales and our space-
427 ground approach can resolve reconnection bursts that are larger than 0.5 Re and persist longer than
428 a few minutes. This is limited by the radar spatial and temporal resolution, and the magnetosphere-
429 ionosphere coupling time which is usually 1-2 min [e.g. Carlson et al., 2004]. This constraint is
430 not expected to impair the result because reconnection bursts above this scale have been found to
431 occur commonly in statistics (see the Introduction section for spatial and Lockwood and Wild
432 [1993], Kuo et al. [1995], Fasel [1995], and McWilliams et al. [1999] for temporal characteristics).

434 3. Observations

435 3.1. Spatially patchy reconnection active at one satellite only

436 3.1.1 In-situ satellite measurements

437 On February 2, 2013, THA and THE made simultaneous measurements of the dayside

461 magnetopause with a 1.9 Re separation in the Y direction around 21:25 UT. The IMF condition is
462 displayed in Figure 1a and the IMF was directed southward. The satellite location in the GSM
463 coordinates is displayed in Figure 1b, and the measurements are presented in Figure 2. The
464 magnetic field and the ion velocity components are displayed in the LMN boundary normal
465 coordinate system, where L is along the outflow direction, M is along the X-line, and N is the
466 current sheet normal. The coordinate system is obtained from the minimum variance analysis of
467 the magnetic field at each magnetopause crossing [Sonnerup and Cahill, 1967]. Figures 2g-p show
468 that both satellites passed from the magnetosheath into the magnetosphere, as seen as the sharp
469 changes in the magnetic field, the ion spectra, and the density (shaded in pink).

470 As THE crossed the magnetopause boundary layer (2122:57-2123:48 UT), it detected both fluid
471 and kinetic signatures of reconnection. It observed a rapid, northward-directed plasma jet within
472 the region where the magnetic field rotated (Figures 2g and 2j). The magnitude of this jet relative
473 to the sheath background flow reached 262 km/s at its peak, which was 72% of the predicted speed
474 of a reconnection jet by the Walen relation (366 km/s, not shown). The angle between the observed
475 and predicted jets was 39°. The ion distributions in Figure 2k showed a distorted D-shaped
476 distribution similar to the finding of by Broll et al., [2018]. The distortion is due to particles
477 traveling in the field-aligned direction from the reconnection site to higher magnetic field region,
478 and Broll et al., [2018] estimated the traveling distance to be a few Re for the observed level of
479 distortion.

480 THA crossed the magnetopause one to two minutes later than THD (2124:48-2125:13 UT).
481 While it still identified a plasma jet at the magnetopause (Figures 2l and 2o), the jet speed was
482 significantly smaller than what was predicted for a reconnection jet (80 km/s versus 380 km/s in
483 the L direction). The observed jet was directed 71° away from the prediction. The ion distributions

507 deviated from clear D-shaped distributions (Figure 2p). Reconnection was thus much less active
508 at THA local time than at THE. This suggests that the X-line of the active reconnection at THE
509 likely did not extend to THA.

511 3.1.2 Ground radar measurements

512 The velocity field of the dayside cusp ionosphere during the satellite measurements is shown in
513 Figures 2a-c. Figure 2a shows the radar LOS measurements at 21:25 UT, as denoted by the color
514 tiles, and the merged vectors, as denoted by the arrows. The colors of the arrows indicate the
515 merged velocity magnitudes, and the colors of the tiles indicate the LOS speeds that direct anti-
516 sunward (those project to the sunward direction appear as black). Fast (red) and anti-sunward flows
517 are the feature of our interest. One such of this flow can be identified in the pre-noon sector, which
518 had a speed of ~800 m/s and was directed poleward and westward. As the merged vector arrows
519 indicate, the velocity vectors have a major component close to the INV beam directions and thus
520 the INV LOS velocities reflect the flow distribution. The flow crossed the open-closed field line
521 boundary, which was located at 78° MLAT based on the spectral width (Figure 2d and S1). This
522 flow thus meets the criteria of being an ionospheric signature of magnetopause reconnection burst.
523 Another channel of fast flow was present in the post-noon sector. This post-noon flow was directed
524 more azimuthally and was separated from the pre-noon flow by a region of slow velocities at >79°
525 MLAT around noon. The two flows are thus two different structures likely originating from two
526 spatially discontinuous reconnection bursts. Since the satellites were located in the pre-noon sector
527 we focus on the pre-noon flow below.

528 The flow had a limited azimuthal extent. The extent is determined at half of the maximum flow
529 speed, which was ~400 m/s. Figure 2f discussed below shows a more quantitative estimate of the

553 extent. In Figure 2a, we mark the eastern and western boundaries with the dashed magenta lines,
554 across which the LOS velocities dropped from red to blue/green colors.

555 Figure 2b shows the SECS velocities, denoted by the arrows. The SECS velocities reasonably
556 reproduced the spatial structure of the flows seen in Figure 2a. The flow boundaries were marked
557 by the dashed magenta lines, across which the flow speed dropped from red to blue. Across the
558 flow western boundary the flow direction also reversed. The equatorward-directed flows are
559 interpreted as the return flow of the poleward flows, as sketched in *Southwood* [1987] and *Oksavik*
560 *et al.* [2004].

561 The velocity field reconstructed using the SHF velocities is shown in Figure 2c (obtained through
562 the Radar Software Toolkit (<http://superdarn.thayer.dartmouth.edu/software.html>)). This is an
563 expanded view of the global convection maps in Figure S2 focusing on the dayside cusp.
564 Comparing Figures 2c and S2 reveals that the employed radars listed in Section 2 have contributed
565 to the majority of the backscatters on the dayside. This is because this event (same for the following
566 two events) occurred under non-storm time, where the open-closed field line was confined within
567 the utilized few radar FOVs. During storm time the boundary expands to lower latitude where
568 backscatter from a wider network of radars may be available. The SHF velocities also captured the
569 occurrence of two flows in the pre- and post-noon sectors, respectively, although the orientation
570 of the flows were less azimuthally-aligned than Figure 2a or 2b. The difference is likely due to the
571 contribution from the statistical potential distribution under the southward IMF. The flow western
572 and eastern boundaries were again marked by the dashed magenta lines.

573 Figure 2d shows spectral width measurements. Large spectral widths can be produced by soft
574 (~100 eV) electron precipitation [*Ponomarenko et al.*, 2007] such as precipitation along
575 reconnected magnetic flux tube, and evidence has shown that the longitudinal extent of large

599 spectral widths correlates with the extent of PMAFs [Moen et al., 2000] and of poleward flows
600 across the OCB [Pinnock and Rodger, 2001]. Large spectral widths thus have the potential to
601 reveal the reconnection burst extent. For the specific event under examination, the region of large
602 spectral widths, appearing as red color, spanned from 10.5 to 14.5 h MLT if we count the sporadic
603 scatters in the post-noon sector. This does not contradict the flow width identified above because
604 the wide width reflects the summed width of the pre- and post-noon flows. In fact a more careful
605 examination shows the presence of two dark red (>220 m/s spectral width) regions embedded
606 within the ~200-m/s spectral widths (circled in red, the red dashed line is due to the discontinuous
607 backscatters outside the INV FOV), corresponding to the two flows.

608 Figures 2a-c all observed a channel of fast anti-sunward flow in the pre-noon sector of the high
609 latitude ionosphere, and the flow had a limited azimuthal extent. If the flow corresponded to
610 magnetopause reconnection, the reconnection burst is expected to span over a limited local time
611 range. This is consistent with the THEMIS satellite observation in Section 3.1.1, where THE at Y
612 = -2.9 Re detected clear reconnection signatures, while THA at Y = -4.8 Re did not. In fact, if we
613 project the satellite location to the ionosphere through field line tracing under the T89 model, THE
614 was positioned at the flow longitude, while THA was to the west of the flow embedded in weak
615 convection (Figure 2a).

616 While this paper primarily focuses on the spatial extent of reconnection bursts, the temporal
617 evolution of reconnection can be obtained from the time series plot in Figure 2e. Figure 2e presents
618 the INV LOS measurements along 80° MLAT (just poleward of the open-closed field line
619 boundary with good LOS measurements) as functions of magnetic longitude (MLON) and time.
620 Similar to the snapshots, the color represents LOS speeds that project to the anti-sunward direction,
621 and the flow of our interest appears as a region of red color. The time and the location where THA

645 and THE crossed the magnetopause are marked by the vertical and horizontal lines. The flow
646 emerged from a weak background at 2120 UT and persisted for ~30 min in INV FOV. At the onset
647 the flow eastern boundary was located at -82° MLON, and interestingly, this boundary spread
648 eastward with time in a similar manner as events studied by Zou et al. [2018]. The flow western
649 boundary was located around -77° MLON during 2120-2134 UT, and started to spread eastward
650 after 2134 UT. Hence the reconnection-related ionospheric flow, once formed, has spread in width
651 and displaced eastward. The spreading has also been noticed in the other two events (see Section
652 3.3), indicating that this could be a common development feature of the reconnection-related flows.
653 The spreading was fast in the first 6 min and then slowed down stabilizing at a finite flow extent
654 until the eastern boundary went outside FOV at 2134 UT.

655 A consequence of the flow temporal evolution is that THA, which was previously outside the
656 reconnection-related flow, became immersed in the flow from 2130 UT, while THE, which was
657 previously inside the flow, was left outside from 2142 UT (Figure 2e). This implies that at the
658 magnetopause the reconnection has spread azimuthally sweeping across THA, and has slid in the
659 $-y$ direction away from THE. This is in perfect agreement with satellite measurements shown in
660 Figures 2q-z. Figures 2q-z presents subsequent magnetopause crossings made by THA and THE
661 following the crossings in Figures 2g-p. THA detected an Alfvénic reconnection jet and a clear D-
662 shape ion distribution, and THE detected a jet much slower than the Alfvénic speed and an ion
663 distribution without a clear D-shape. This corroborates the connection between the in-situ
664 reconnection signatures with the fast anti-sunward ionospheric flow, and reveals the dynamic
665 evolution of reconnection in the local time direction.

666 We quantitatively determine the flow extent in Figure 2f. Figure 2f shows the INV LOS velocity
667 profile at 2125 UT as a function of magnetic longitude and distance from 0° MLON. The 2125 UT

691 is the same time instance as in Figures 2a-c and is the time when the flow extent has slowed down
692 from spreading and stabilized. The profile is taken along 80° MLAT. While this latitude is 2°
693 poleward of the open-closed field line boundary, the shape of the flow did not change much over
694 the 2° displacement and thus still presents the reconnection extent. The flow velocity profile has a
695 skewed Gaussian shape, and we quantify the flow azimuthal extent as the full-width-at-half-
696 maximum (FWHM). The FWHM was 13° in MLON or 260 km at an altitude of 260 km. Also
697 shown is the SECS velocity profile. Here we only show the northward component of the SECS
698 velocity as this component represents reconnecting flows across an azimuthally-aligned open-
699 closed field line boundary. The SECS velocity profile gives a FWHM of 13.5° in MLON or 270
700 km, very similar to the LOS profile.

701 It is noteworthy mentioning that the velocity profile obtained above approximates to the profile
702 of reconnection electric field along the open-closed field line boundary (details in Figure S3).
703 Reconnection electric field can be estimated by measuring the flow across the open-closed field
704 line boundary in the reference frame of the boundary [Pinnock *et al.*, 2003; Freeman *et al.*, 2007;
705 Chisham *et al.*, 2008]. However, a precise determination of the boundary motion is subject to radar
706 spatial and temporal resolution and for a slow motion like the events studied in this paper (Figure
707 S1), the signal to noise ratio is lower than one. For this reason this paper focuses on the velocity
708 profile poleward of the open-closed field line boundary, which is less affected by the error
709 associated with the boundary.

710 To infer the reconnection burst extent at the magnetopause, we project the flow width in the
711 ionosphere to the equatorial plane. The result suggests that the reconnection local time extent was
712 ~3 Re.

713 Before closing this section, we would like to point out that the determined extent is characterized

714 by the FWHM of the fast anti-sunward ionospheric flow, which allows weak flows to extend
715 beyond the flow extent. When THA and THE were positioned within the weak flows in the
716 ionosphere, they at the magnetopause observed flows much weaker than the Walen prediction.
717 This may imply that there were two components of reconnection at different scales in this event:
718 weak background reconnection signified by the slow flows, and embedded strong reconnection
719 bursts signified by the fast flows.

720 3.1.1. In situ satellite measurements

721 On March 11, 2014, THA and THD made simultaneous measurements of the dayside
722 magnetopause with a 4.2 Re separation in the Y direction. The IMF condition is displayed in Figure
723 1a and the IMF was directed southward. The satellite location in the GSM coordinates is displayed
724 in Figure 1b, and the measurements are presented in Figures 1c–h. The magnetic field and the ion
725 velocity components are displayed in the LMN boundary normal coordinate system, where *L* is
726 along the outflow direction, *M* is along the X line, and *N* is the current sheet normal. The
727 coordinate system is obtained from the minimum variance analysis of the magnetic field at each
728 magnetopause crossing [Sonnerup and Cahill, 1967]. Both satellites passed from the
729 magnetosphere into the magnetosheath, as seen as the sharp changes in the magnetic field, the ion
730 spectra, and the density (shaded in pink).

731 As THD crossed the magnetopause boundary layer (1624:47–1625:09 UT), it detected both fluid
732 and kinetic signatures of reconnection. It observed a rapid, northward directed plasma jet within
733 the region where the magnetic field rotated (Figures 1e and 1f). The magnitude of this jet reached
734 138 km/s at its peak, which was 60% of the predicted speed of a reconnection jet by the Walen
735 relation (231 km/s, not shown). The angle between the observed and predicted jets was 22°. The
736 jet velocity was somewhat small (although still sufficiently large that $\Delta V^* > 0.5$) because of the

737 presence of cold magnetospheric ions seen in Figure 1g [Phan *et al.*, 2013]. Figure 1g suggests
738 that the magnetosheath ion population had a parallel velocity of ~ 200 km/s, and the cold
739 magnetospheric ion population had a parallel velocity near zero. Therefore although the bulk
740 velocity computed by combining the two populations was considerably slower than the Walen
741 prediction, the velocity of the magnetosheath population was actually very close to the prediction.
742 The ion distributions in Figure 1g showed a characteristic D-shaped distribution, consistent with
743 active reconnection.

744 THA crossed the magnetopause one minute earlier than THD (1623:29–1624:07 UT). While it
745 still identified a plasma jet at the magnetopause (Figures 1h and 1k), the jet speed was significantly
746 smaller than what was predicted for a reconnection jet (97 km/s versus 200 km/s). The observed
747 jet was directed 21° away from the prediction. No clear D-shaped distributions have been found
748 in the ion distributions at the magnetopause (Figure 1l). Reconnection was thus much less active
749 at THA local time than at THD. This suggests that the X-line of the active reconnection at THD
750 likely did not extend to THA.

751

752 3.1.2 Ground radar measurements

753 The velocity field of the dayside cusp ionosphere during the satellite measurements is shown in
754 Figure 2 (the 1 min difference from the satellite magnetopause crossing time is negligible as it was
755 within the 1–2 min radar resolution). Figure 2a shows the radar LOS measurements, as denoted by
756 the color tiles, and the merged vectors, as denoted by the arrows. The colors of the arrows indicate
757 the merged velocity magnitudes, and the colors of the tiles indicate the LOS speeds that direct anti-
758 sunward (those project to the sunward direction appear as black). Fast (red) and anti-sunward flows
759 are the feature of our interest. One channel of such flow can be identified in the pre-noon sector,

760 which had a speed of ~ 700 m/s and was directed poleward and westward. The velocity
761 vectors $\gg 80^\circ$ MLAT were directed roughly parallel to the RKN radar beams, and therefore the
762 RKN LOS measurements represent the primary component of the flow. The flow crossed the open-
763 closed field line boundary, which stayed quasi-steadily at 77° MLAT based on the spectral width
764 (Figure 2d discussed below). This flow thus meets the criteria of being an ionospheric signature
765 of magnetopause reconnection.

766 The flow had a limited azimuthal extent. The extent is determined at half of the maximum flow
767 speed, which was ~ 400 m/s. Figure 2e discussed below shows a more quantitative estimate of the
768 extent. In Figure 2a, we mark the eastern boundary with the dashed magenta line, across which the
769 velocity vectors at 79° – 83° MLAT dropped from red/orange to green color. Those green vectors,
770 different from the red vectors, were directed mainly westward roughly in parallel to the CLY radar
771 beams. They had a small poleward velocity component, or even an equatorward component, up to
772 2 h in MLT past magnetic noon as seen from the dark blue and the black LOS measurements from
773 RKN and SAS. They hence were the slow background convection outside the fast anti-sunward
774 flow. The western boundary of the flow had extended beyond the RKN FOV. But it did not extend
775 more than 1.5 h in MLT beyond because the INV echoes there showed weakly poleward and
776 equatorward LOS speeds across the open-closed field line boundary.

777 It is possible to infer the location of the flow western boundary more definitively from the SECS
778 velocities than the LOS measurements. Figure 2b shows the SECS velocities, denoted by the
779 arrows. The SECS velocities reasonably reproduced the spatial structure of the flow channel seen
780 in Figure 2a. The flow western boundary was marked by the dashed magenta line, across which
781 the flow speed dropped and the flow direction reversed. The equatorward-directed flows are
782 interpreted as the return flow of the poleward flows, as sketched in *Southwood* [1987] and *Oksavik*

783 *et al.* [2004].

784 The velocity field reconstructed using the SHF velocities is shown in Figure 2c (obtained
785 through the Radar Software Toolkit (<http://superdarn.thayer.dartmouth.edu/software.html>)). The
786 SHF velocities also exhibit a channel of fast poleward and westward directed flow, which was
787 similar to the flow channel in Figure 2b. The flow western and eastern boundaries were again
788 marked by the dashed magenta lines (using the same ~400 m/s threshold as above), across which
789 the SHF velocities dropped from orange to green/blue.

790 We can test the reliability of the identified flow extent by referring to the extent of the cusp.
791 Evidence has shown that the longitudinal extent of the cusp correlates with the extent of PMAFs
792 [Moen *et al.*, 2000] and of poleward flows across the open-closed field line boundary [Pinnock
793 and Rodger, 2001]. Figure 2d shows spectral width measurements and the cusp can be identified
794 as a region of high spectral widths (red color) as circled in the red contour. The cusp was located
795 at the western half of the RKN FOV and its eastern edge corresponded to a drop of the spectral
796 widths from red to green color. The western edge extended beyond the RKN FOV and the
797 extension was partially captured by the PGR echoes (marked by the dashed line as the backscatters
798 there had gaps in space and were sporadic in time). But it ended around the low spectral widths of
799 the CLY backscatters eastward of the INV FOV. The location and the extent of the cusp therefore
800 support the location and the extent of the anti-sunward flow.

801 The limited extent of the flow did not vary much in time, as suggested by the time series plot in
802 Figure 2e. Figure 2e presents the RKN LOS measurements along 80° MLAT as functions of
803 magnetic longitude (MLON) and time. Similar to the snapshots, the color represents LOS speeds
804 that project to the anti-sunward direction, and the flow of our interest appears as a region of red
805 color. The time when THA and THD crossed the magnetopause was marked by the red arrows.

806 The fact that the flow channel stayed quasi-steady during the satellite conjunction period suggests
807 that the satellite measurements in Section 3.1.1 reflect the spatial distribution, rather than the
808 temporal variation, of reconnection.

809 Figures 2a-c all observed a channel of fast anti-sunward flow in the pre-noon sector of the high
810 latitude ionosphere, and the channel had a limited azimuthal extent. If the flow corresponded to a
811 magnetopause reconnection, the X-line is expected to be located in the GSM $Y < 0$ regime and
812 spans over a limited local time range. This is consistent with the THEMIS satellite observation in
813 Section 3.1.1, where THD at $Y = -2.0 R_E$ detected clear reconnection signatures, while THA at Y
814 $= -2.2 R_E$ did not. In fact, if we project the satellite location to the ionosphere through field line
815 tracing under the T89 model, THD was positioned close to the flow eastern boundary, while THA
816 was far away (Figures 2a-c).

817 The radar observations thus provide critical information to interpret the in-situ reconnection
818 extent. The X-line detected by THD did not extend duskward passing through the subsolar point
819 of the magnetosphere; instead it extended dawnward towards the dawnside magnetopause. Note
820 that the observations presented here do not rule out existence of other X-lines along the
821 magnetopause, as there might exist other fast anti-sunward flows outside the radar FOVs. But those
822 X-lines are not the focus of this study. It should also be noted that the determined flow extent is
823 based on half of the maximum flow speed, which allows weak anti-sunward flows to extend
824 beyond the flow boundaries. The weak flows are expected to correspond to weak background
825 reconnection at the magnetopause. In fact, THA had detected weak reconnection signatures (i.e.
826 weak plasma jets) $4 R_E$ eastward of the active reconnection signatures at THD as found in Section
827 3.1.1, and this may agree with the weak ionospheric convection (green vectors in Figures 2a-c)
828 eastward of the flow channel.

829 We quantitatively determine the flow extent in Figure 2f. Figure 2f shows the RKN LOS
830 velocity profile along 80° MLAT at 1624 UT (the same time as Figures 2a-c) as a function of
831 magnetic longitude and distance from 0° MLON. As mentioned above, the RKN LOS
832 measurements captured the flow major component and thus approximated to the true 2-d velocities.
833 Also shown is the SECS velocity profile. Here we only show the northward component of the
834 SECS velocity as this component represents reconnecting flows across an azimuthally aligned
835 open-closed field line boundary. We quantify the flow azimuthal extent as the full width at half-
836 maximum (FWHM) of the velocity profile. But the LOS measurements only captured part of the
837 flow channel, and could only reveal the half width at half maximum (HWHM) on one side of the
838 velocity profile. The HWHM was 15° in MLON and 300 km at an altitude of 250 km. The SECS
839 velocities covered the entire flow channel, and can be used to determine the FWHM. The FWHM
840 was 26° in MLON and 520 km.

841 To infer the X-line extent at the magnetopause, we project the flow width in the ionosphere to
842 the equatorial plane. This is done by mapping a pair of ionospheric locations that are azimuthally
843 separated around the THD footprint to the equatorial plane. The ratio of the pair separation in the
844 equatorial plane to that in the ionosphere gives a mapping factor. The mapping factor under T89
845 is 55, and this suggests the X-line local time extent to be ~ 4 Re.

846

847 3.2. Spatially patchy reconnection active at both satellites

848 3.2.1. In-situ satellite measurements

849 On April 19, 2015, under a southward IMF (Figure 3a), THA and THE crossed the
850 magnetopause nearly simultaneously (< 2 min lag) with a 0.5 Re separation in Y (Figure 3b). They
851 passed from the magnetosheath into the magnetosphere. Both satellites observed jets in the VL

852 component at the magnetopause ([Figures 4g-p](#)). The jet at THA at ~1828:05 UT had a speed of
853 84% of and an angle within $\sim 15^\circ$ from the Walen prediction. The jet at THE at ~1826:25 UT had
854 a speed of 95% of and an angle of $\sim 29^\circ$ from the Walen prediction. The ion distributions at THA
855 and THE exhibit clear D-shaped distributions, indicative of active reconnection at these two local
856 times.

857

858 Section 3.2.2. Ground radar measurements

859 During the satellite measurements, the radars observed a channel of fast anti-sunward flow
860 around magnetic noon ([Figures 4a-c](#)). The flow crossed the open-closed field line boundary at 77°
861 MLAT, and qualifies for an ionospheric signature of magnetopause reconnection [burst](#). The flow
862 direction was nearly parallel to the RKN radar beams, and therefore the RKN LOS measurements
863 in [Figure 4a](#) approximated to the 2-d flow speed. The flow eastern boundary can be identified as
864 where the velocity dropped from red/orange to blue (dashed magenta line). Determining the flow
865 western boundary requires more measurements of the background convection velocity, which is
866 beyond the RKN FOV. But we [again](#) infer that the western boundary did not extend more than 1.5
867 h westward beyond the RKN FOV because the PGR and INV echoes there showed weakly
868 poleward and equatorward LOS speeds around the open-closed field line boundary. The CLY radar
869 data further indicated that the anti-sunward flow had started to rotate westward immediately
870 beyond the RKN FOV. This is because the CLY LOS velocities measured between the RKN and
871 INV radar FOVs were larger for more east-west oriented beams (appearing as yellow color) than
872 for more north-south oriented beams (green color). The rotation likely corresponds to the vortex
873 at the flow western boundary as sketched in *Oksavik et al. [2004]*.

874 The more precise location of the western boundary can be retrieved from the SECS velocities

875 in Figure 4b and the SHF velocities in Figure 4c. The SECS velocities present a flow channel very
876 similar to that in Figure 4a, while the flow channel in the SHF velocities was more azimuthally-
877 aligned than in Figures 4a-b.

878 The determined flow extent agrees with the extent of the cusp in Figure 4d. The high spectral
879 widths associated with the cusp were located at the western half of the RKN FOV. They extended
880 westward beyond the RKN FOV into CLY far range gates, where they dropped from red to green
881 color. This is consistent with the inferred location and extent of the anti-sunward flow.

882 The flow of our interest just emerged from a weak background at the time when the THEMIS
883 satellites crossed the magnetopause (Figure 4e). This implies that the related reconnection burst
884 just initiated at the studied local time. The flow and the reconnection burst remained with a roughly
885 steady and localized extent after formation. We quantify the half width at half maximum (HWHM)
886 of the flow using the RKN LOS velocity profile at 0830 UT (Figure 4f), and the HWHM was 10°
887 MLON and 220 km. The FWHM is determined using the SECS velocities, and the FWHM was
888 26° MLON and 572 km. Such an FWHM corresponds to ~5 Re in the equatorial plane.

889 The fact that the fast anti-sunward flow had a limited azimuthal extent around magnetic noon
890 implies that the corresponding magnetopause reconnection burst X-line should span over a limited
891 local time range around the noon. This is consistent with the THEMIS satellite observation in
892 Section 3.2.1, where reconnection was active at Y = 0.7 (THA) and 0.2 Re (THE). Projecting THA
893 and THE locations to the ionosphere reveals that both satellite footprints were located within the
894 flow longitudes. Therefore the reconnection at the two satellites was part of the same ~~X-~~
895 reconnection burst around the subsolar point of the magnetopause. (The THE footprint was
896 equatorward of THA because the X location of THE was closer to the Earth than THA. The
897 magnetopause was expanding and it swept across THE and then THA.) The ~~X-line~~ reconnection

921 further extended azimuthally beyond the two satellite locations, reaching a full length of ~ 5 Re.

922

923 3.3. Spatially continuous and extended reconnection active at both satellites

924 3.3.1. In-situ satellite measurements

925 On Apr 29, 2015, under a prolonged and steady southward IMF ([Figure 5a](#)), THA and THE
926 crossed the magnetopause successively with a time separation of ~ 30 min. The locations of the
927 crossings were separated by 0.1-0.2 Re in the Y direction (Figure 5b). The satellites passed from
928 the magnetosphere into the magnetosheath, and the magnetic field data suggest that the satellites
929 crossed the current layer multiple times before completely entering the magnetosheath ([Figures](#)
930 [6i-r](#)). We therefore only display the magnetic field and the plasma velocity in the GSM coordinates.
931 Both satellites detected multiple flow jets, all agreeing with the Walen prediction with $\Delta V^* > 0.5$.
932 For example, the jet at 1849-1850 UT measured by THA had a speed with 80% of and angle with
933 9° from the Walen prediction, and the jet at 1920-1922 UT by THE had a speed with 83% of and
934 an angle with 1° from the Walen prediction. The ion distributions at THA and THE exhibit clear
935 D-shaped distributions. Such observations suggest that reconnection was active at the THA and
936 THE local times.

937

938 3.3.2. Ground radar measurements

939 In the ionosphere, the radars detected a fast anti-sunward flow as an ionospheric signature of
940 the magnetopause reconnection [burst](#) (Figures 6a-c). The flow velocity here had a large component
941 along the looking directions of the INV and CLY radars, and we therefore focus on the LOS
942 measurements of these two radars. The flow had a broad azimuthal extent, as delineated by the
943 dashed magenta lines (Figure 6a). A similar flow distribution is found in the SECS velocities

Formatted

944 (Figure 6b), and the SHF velocities (Figure 6c). Corresponding to the broad extent of the flow, the
945 cusp had a broad extent (Figure 6d). The cusp continuously spanned across the INV and RKN
946 FOVs and its western and eastern edges coincided with the western and eastern boundaries of the
947 flow, supporting our delineation of the flow extent.

948 The wide flow channel in the ionosphere implies that the corresponding magnetopause ~~X~~
949 ~~linereconnection burst~~ should be wide in local time. Based on the flow distribution, we infer that
950 much of the ~~X~~ linereconnection burst should be located on the pre-noon sector, except that the
951 eastern edge can extend across the magnetic noon meridian to the early post-noon sector. This
952 inference is again consistent with the inference from the THA and THE measurements that the
953 reconnection burst extended at least over the satellite separation ($Y = -0.2$ (THA) and 0 Re (THE)).
954 Note, however, that the distance between THA and THE only covered $<2\%$ of the ~~X~~
955 ~~linereconnection burst~~ extent determined from the ionosphere flow. While the satellite
956 configuration and measurements here were similar to those in Section 3.2, the extent of
957 reconnection bursts was fundamentally different. This suggests that it is difficult to obtain a
958 reliable estimate of the reconnection burst extent without the support of 2-d measurements and that
959 satellites alone also cannot differentiate spatially extended reconnection from spatially patchy
960 reconnection.

961 The flow temporal evolution is shown in Figures 6e-f, where the velocities are based on the LOS
962 measurements from the CLY (Figure 6e) and INV (Figure 6f) radars. The velocities $>-18^\circ$ MLON
963 are not useful and are shaded in grey. These measurements were from short range gates of the CLY
964 radar, where the convection velocity is underestimated as the Doppler velocity is limited below
965 the ion acoustic speed (~ 400 m/s) [Haldoupis, 1989; Koustov et al., 2005]. An overall wide flow
966 channel is seen between $\sim -90^\circ$ and -30° MLON for most of the studied time period, and in

967 particular the flow azimuthal extent were nearly identical at the instances when THA and THE
968 observed the reconnection. But between the two satellite observations, the flow experienced an
969 interesting variation. The velocity at -74° – -30° MLON dropped by 100-200 m/s during 1900-1910
970 UT, while the velocity at -88° – 74° MLON did not change substantially. The velocity enhanced
971 again from 1910 UT. The enhancement first occurred at $\sim -60^{\circ}$ – -40° MLON and then spread
972 azimuthally towards east and west. The enhancement spread by 18° over 14 min at its eastern end
973 (marked by the dashed magenta line), suggesting a spreading speed of 429 m/s. The spreading at
974 the western end soon merged with the velocity enhancement at -88° – 74° MLON, but a rough
975 estimate suggests a speed of 444 km/s. It should be noted that the all three components of the IMF
976 stayed steady for an extended time (Figure 7, discussed below in Section 3.4), and thus the
977 evolution of the flow/reconnection was unlikely to be externally driven.

978 This sequence of changes gives an important implication that the spatially extended
979 reconnectionX-line was a result of spreading of an initially patchy reconnectionX-line. If we map
980 the spreading in the ionosphere to the magnetopause, the spreading occurred bi-directionally and
981 at a speed of 24 km/s in each direction based on field-line mapping under the T89 model (the
982 mapping factor was 55). The spreading process persisted for 10-20 min. Such an observation is
983 similar to what has recently been reported by *Zou et al.* [2018], where the X-linesreconnection also
984 spreads bi-directionally at a speed of a few tens of km/s. However, the spreading in *Zou et al.*
985 [2018] occurs following a southward turning of the IMF, while the spreading here occurred without
986 IMF variations. The mechanism of spreading is explained either as motion of the current carriers
987 of the reconnecting current sheet or as propagation of the Alfvén waves along the guide field [*Huba*
988 *and Rudakov*, 2002; *Shay et al.* 2003; *Lapenta et al.*, 2006; *Nakamura et al.*, 2012; *Jain et al.*,
989 2013].

990 It should be noted that ~~X-line~~reconnection spreading can be a common process of reconnection
991 that is not limited to extended ~~X-lines~~reconnection. A careful examination of Figure 4d suggests
992 that spreading may have also occurred for the spatially patchy ~~reconnection~~X-line (the eastern
993 limit of the red/orange region spread from -36° to -29° MLON during 1828-1832 UT). The two
994 ~~X-lines~~reconnection spread at a similarly speed, but duration of the spreading process was two to
995 three times longer in the spatially extended than the spatially patchy reconnection events.

996 Figures 6g-h quantify the FWHM of the fast anti-sunward flow around the time when THA and
997 THE measured active reconnection. The width can be obtained based on the LOS measurements,
998 where we determine the HWHMs of the flow in the INV and CLY FOVs separately and add them
999 together as the FWHM. The FWHM was 63° MLON and 1260 km when THA measured the
1000 reconnection, and was 62° MLON and 1240 km when THE measured the reconnection. This
1001 corresponds to ~~an X-line length~~a reconnection burst extent of ~ 11 Re. Note that the determination
1002 of the HWHM inside the CLY FOV has taken into account a background convection of ~ 400 m/s.
1003 The background came from those plasmas moving azimuthally along the open-closed field line
1004 boundary but not crossing the boundary. The width can also be obtained based on the SECS
1005 measurements, which was 64° MLON and 1280 km when THA measured the reconnection, and
1006 60° MLON and 1200 km when THE measured the reconnection. This is very close to the values
1007 derived from the LOS measurements.

1008

1009 3.4. IMF and solar wind conditions for spatially patchy and extended reconnection

1010 The above events definitely show that the local time extent of magnetopause reconnection ~~X-~~
1011 linesbursts can vary from a few to >10 Re. Here we investigate whether and how the extent may
1012 depend on the upstream driving conditions. Figure 7 presents the IMF, the solar wind velocity, and

1036 the solar wind pressure taken from the OMNI data for the three events. The red vertical lines mark
1037 the times when the reconnection was measured. The three events occurred under similar IMF field
1038 strengths (5-6 nT), similar IMF Bz components (-2-3 nT), and similar ~~solar wind velocities (300-~~
1039 ~~400 km/s) and~~ dynamic pressures (1-2 nPa), implying that the different ~~X-line~~ reconnection burst
1040 extents were unlikely due to these parameters. The solar wind speeds were also similar among the
1041 three events, the speed being slightly larger for the spatially patchy than extended reconnection.
1042 This is different from *Milan et al.* [2016], who identified the solar wind velocity as the controlling
1043 factor of reconnection burst extent, where a larger solar wind speed causes a larger reconnection
1044 burst extent. However, *Milan et al.* [2016] studied reconnection under very strong IMF driving
1045 conditions when $|B| \sim 15$ nT, while our events occurred under a more typical moderate driving ($|B|$
1046 $\sim 5-6$ nT).

1047 The spatially patchy reconnection ~~X-line~~ events had an IMF Bx of a larger magnitude than the
1048 extended reconnection event did (4 vs. 0 nT). The spatially patchy reconnection ~~X-line~~ events also
1049 had an IMF By component of a smaller magnitude (2 vs. 5 nT), and with more variability on time
1050 scales of tens of minutes, than the extended ~~X-line~~ reconnection event. The IMF Bx and By
1051 components are known to modify the magnetic shear across the magnetopause and to affect the
1052 occurrence location of reconnection. Studies have found that small $|B_y|/|B_z|$ relates to anti-
1053 parallel and large $|B_y|/|B_z|$ to component reconnection [Coleman et al., 2001; Chisham et al.,
1054 2002; Trattner et al., 2007]. Large $|B_x|/|B|$, i.e. cone angle, also favors formation of high-speed
1055 magnetosheath jets [Archer and Horbury, 2013; Plaschke et al., 2013] of a few Re in scale size,
1056 resulting in a turbulent magnetosheath environment for reconnection to occur [Coleman, and
1057 Freeman, 2005]. The steady IMF condition may allow ~~X-lines~~ reconnection to spread across local
1058 times unperturbedly, eventually reaching a wide extent. Thus the ~~X-line~~ reconnection burst extent

1059 may depend on the IMF orientation and steadiness, although whether and how they influence the
1060 extent needs to be further explored.

1061

1062 4. Summary

1063 We carefully investigate the local time extent of magnetopause reconnection ~~X-lines~~bursts by
1064 comparing the measurements of two THEMIS satellites and three ground radars. The radars
1065 identify signatures of reconnection bursts as fast ionospheric flows moving anti-sunward across
1066 the open-closed field line boundary. When reconnection is active at only one of the two satellite
1067 locations, only the ionosphere conjugate to this spacecraft shows a channel of fast anti-sunward
1068 flow. When reconnection is active at both spacecraft and the spacecraft are separated by <1 Re,
1069 the ionosphere conjugate to both spacecraft shows a channel of fast anti-sunward flow. The fact
1070 that the satellite locations are mapped to the same flow channel suggests that the ~~X-~~
1071 ~~line~~reconnection is continuous between the two satellites, and that it is appropriate to take the
1072 satellite separation as a lower limit estimate of the ~~X-line~~reconnection burst extent. Whether ~~the~~
1073 ~~X-line~~reconnection can still be regarded as continuous when the satellites are separated by a few
1074 or > 10 Re is questionable, and needs to be examined using conjunctions with a larger satellite
1075 separation than what have been presented here.

1076 The ~~X-line~~reconnection burst extent is measured as the extent of the ionospheric flow. In the
1077 three conjunction events, the flows have an extent of ~~520~~260, 572, and 1260 km in the ionosphere,
1078 which corresponds to ~~~4~~3, 5, and 11 Re at the magnetopause (under the T89 model) in the local
1079 time direction. This provides strong observational evidence that magnetopause reconnection bursts
1080 can occur over a wide range of extents, from spatially patchy (a few Re) to spatially continuous
1081 and extended (>10 Re). Interestingly, the extended reconnection is seen to initiate from a patchy

1105 reconnection, where the ~~X-line~~reconnection grows by spreading across local time. The speed of
1106 spreading is 50 km/s summing the westward and eastward spreading motion, and the spreading
1107 process persists for 10-20 min.

1108 The ~~X-line~~reconnection burst extent may be affected by the IMF orientation and steadiness,
1109 although the mechanism is not clearly known. For the modest solar wind driving conditions studied
1110 here, the spatially extended reconnection ~~X-line~~ occurs under a smaller IMF B_x component, and a
1111 larger and steadier IMF B_y component than the spatially patchy reconnection~~X-line~~. The IMF
1112 strength, the B_z component, and the solar wind velocity and pressure are about the same for the
1113 extended and the patchy reconnection~~X-lines~~. Reconnection can vary with time, even under steady
1114 IMF driving conditions.

1115

1116 **Acknowledgments.** This research was supported by the NASA Living With a Star Jack Eddy
1117 Postdoctoral Fellowship Program, administered by UCAR's Cooperative Programs for the
1118 Advancement of Earth System Science (CPAESS), NASA grant NNX15AI62G, NSF grants PLR-
1119 1341359 and AGS-1451911, and AFOSR FA9550-15-1-0179 and FA9559-16-1-0364. The
1120 THEMIS mission is supported by NASA contract NAS5-02099. SuperDARN is a collection of
1121 radars funded by national scientific funding agencies. SuperDARN Canada is supported by the
1122 Canada Foundation for Innovation, the Canadian Space Agency, and the Province of
1123 Saskatchewan. We thank Tomoaki Hori for useful discussion on the SECS technique. Data
1124 products of the SuperDARN, THEMIS, and OMNI are available at <http://vt.superdarn.org/>,
1125 <http://themis.ssl.berkeley.edu/index.shtml>, and GSFC/SPDF OMNIWeb website.

1126

1127 Reference

1151 Amm, O., A. Grocott, M. Lester, and T. K. Yeoman (2010), Local determination of ionospheric
1152 plasma convection from coherent scatter radar data using the SECS technique, *J. Geophys.*
1153 *Res.*, 115, A03304, doi:[10.1029/2009JA014832](https://doi.org/10.1029/2009JA014832).

1154 Alexeev, I. I., D. G. Sibeck, and S. Y. Bobrovnikov (1998), Concerning the location of
1155 magnetopause merging as a function of the magnetopause current strength, *J. Geophys.*
1156 *Res.*, 103(A4), 6675–6684, doi:[10.1029/97JA02863](https://doi.org/10.1029/97JA02863).

1157 Angelopoulos, V. (2008), The THEMIS mission, *Space Sci. Rev.*, 141, 5–34,
1158 doi:[10.1007/s11214-008-9336-1](https://doi.org/10.1007/s11214-008-9336-1).

1159

1160 [Archer M O. Horbury T S. Magnetosheath dynamic pressure enhancements: Occurrence and](#)
1161 [typical properties. *Ann. Geophys.* 2013;31:319–331. doi:10.5194/angeo-31-319-2013.](#)

1162 Auster, H. U., et al. (2008), The THEMIS fluxgate magnetometer, *Space Sci. Rev.*, **141**, 235–
1163 264.

1164 Baker, K. B., J. R. Dudeney, R. A. Greenwald, M. Pinnock, P. T. Newell, A. S. Rodger, N.
1165 Mattin, and C.-I. Meng (1995), HF radar signatures of the cusp and low-latitude boundary
1166 layer, *J. Geophys. Res.*, 100(A5), 7671–7695, doi:[10.1029/94JA01481](https://doi.org/10.1029/94JA01481).

1167 Baker, K. B., A. S. Rodger, and G. Lu (1997), HF-radar observations of the dayside magnetic
1168 merging rate: A Geospace Environment Modeling boundary layer campaign study, *J.*
1169 *Geophys. Res.*, 102(A5), 9603–9617, doi:[10.1029/97JA00288](https://doi.org/10.1029/97JA00288).

1170 [Bobra, M. G., S. M. Petrinec, S. A. Fuselier, E. S. Claflin, and H. E. Spence \(2004\), On the solar](#)
1171 [wind control of cusp aurora during northward IMF, *Geophys. Res. Lett.*, 31, L04805,](#)
1172 [doi:10.1029/2003GL018417.](#)

1173 Borovsky, J. E. (2013), Physical improvements to the solar wind reconnection control function for

1197 the Earth's magnetosphere, *J. Geophys. Res. Space Physics*, 118, 2113–2121,
1198 doi:[10.1002/jgra.50110](https://doi.org/10.1002/jgra.50110).

1199 Bristow, W. A., D. L. Hampton, and A. Otto (2016), High-spatial-resolution velocity
1200 measurements derived using Local Divergence-Free Fitting of SuperDARN observations, *J.*
1201 *Geophys. Res. Space Physics*, 121, 1349–1361, doi:[10.1002/2015JA021862](https://doi.org/10.1002/2015JA021862).

1202 [Chisham, G., I. J. Coleman, M. P. Freeman, M. Pinnock, and M. Lester \(2002\), Ionospheric](#)
1203 [signatures of split reconnection X-lines during conditions of IMF \$B_z < 0\$ and \$|B_y|/|B_z|\$:](#)
1204 [Evidence for the antiparallel merging hypothesis, *J. Geophys. Res.*, 107\(A10\), 1323,](#)
1205 [doi:\[10.1029/2001JA009124\]\(https://doi.org/10.1029/2001JA009124\).](#)

1206 Chisham, G., and Freeman, M. P. (2003): A technique for accurately determining the cusp-
1207 region polar cap boundary using SuperDARN HF radar measurements, *Ann. Geophys.*, 21,
1208 983–996.

1209 [Chisham, G., M. P. Freeman, I. J. Coleman, M. Pinnock, M. R. Hairston, M. Lester, and G.](#)
1210 [Sofko \(2004\), Measuring the dayside reconnection rate during an interval of due northward](#)
1211 [interplanetary magnetic field, *Ann. Geophys.*, 22, 4243–4258,](#)

1212 [Chisham, G., and M. P. Freeman \(2004\), An investigation of latitudinal transitions in the](#)
1213 [SuperDARN Doppler spectral width parameter at different magnetic local times, *Ann.*](#)
1214 [Geophys.](#), 22, 1187–1202.

1215 [Chisham, G., M. P. Freeman, and T. Sotirelis \(2004b\), A statistical comparison of SuperDARN](#)
1216 [spectral width boundaries and DMSP particle precipitation boundaries in the nightside](#)
1217 [ionosphere, *Geophys. Res. Lett.*, 31, L02804, doi:\[10.1029/2003GL019074\]\(https://doi.org/10.1029/2003GL019074\).](#)

1218 [Chisham, G., M. P. Freeman, T. Sotirelis, R. A. Greenwald, M. Lester, and J.-P. Villain \(2005a\),](#)
1219 [A statistical comparison of SuperDARN spectral width boundaries and DMSP particle](#)

1243 [precipitation boundaries in the morning sector ionosphere, *Ann. Geophys.*, 23,733–743.](#)

1244 [Chisham, G., M. P. Freeman, T. Sotirelis, and R. A. Greenwald \(2005b\), The accuracy of using](#)

1245 [the spectral width boundary measured in off-meridional SuperDARN HF radar beams as a](#)

1246 [proxy for the open-closed field line boundary, *Ann. Geophys.*, 23, 2599–2604.](#)

1247 [Chisham, G., M. P. Freeman, M. M. Lam, G. A. Abel, T. Sotirelis, R. A. Greenwald, and M.](#)

1248 [Lester \(2005c\), A statistical comparison of SuperDARN spectral width boundaries and](#)

1249 [DMSF particle precipitation boundaries in the afternoon sector ionosphere, *Ann. Geophys.*,](#)

1250 [23, 3645–3654.](#)

1251 [Chisham, G., et al. \(2008\), Remote sensing of the spatial and temporal structure of magnetopause](#)

1252 [and magnetotail reconnection from the ionosphere, *Rev. Geophys.*, 46, RG1004,](#)

1253 [doi:10.1029/2007RG000223.](#)

1254 [Coleman, I. J., G. Chisham, M. Pinnock, and M. P. Freeman \(2001\), An ionospheric convection](#)

1255 [signature of antiparallel reconnection, *J. Geophys. Res.*, 106, 28,995–29,007.](#)

1256 [Coleman, I. J., and M. P. Freeman \(2005\), Fractal reconnection structures on the magnetopause,](#)

1257 [Geophys. Res. Lett., 32, L03115, doi:10.1029/2004GL021779.](#)

1258 Cousins, E. D. P., and S. G. Shepherd (2010), A dynamical model of high - latitude convection

1259 derived from SuperDARN plasma drift measurements, *J. Geophys. Res.*, 115, A12329,

1260 doi:10.1029/2010JA016017.

1261 Crooker, N. U. (1979), Dayside merging and cusp geometry, *J. Geophys. Res.*, 84(A3), 951–959,

1262 doi:10.1029/JA084iA03p00951.

1263 Crooker, N. U., F. R. Toffoletto, and M. S. Gussenhoven (1991), Opening the cusp, *J. Geophys.*

1264 *Res.*, 96(A3), 3497–3503, doi: 10.1029/90JA02099.

1265 Denig, W. F., W. J. Burke, N. C. Maynard, F. J. Rich, B. Jacobsen, P. E. Sandholt, A. Egeland, S.

Formatt

Formatt

Formatt

Formatt

Formatt

Formatt

Formatt

Formatt

- 1289 Leontjev, and V. G. Vorobjev (1993), Ionospheric signatures of dayside magnetopause
1290 transients: A case study using satellite and ground measurements, *J. Geophys.*
1291 *Res.*, **98**(A4), 5969–5980, doi:[10.1029/92JA01541](https://doi.org/10.1029/92JA01541).
- 1292 Dorelli, J. C., A. Bhattacharjee, and J. Raeder (2007), Separator reconnection at Earth's dayside
1293 magnetopause under generic northward interplanetary magnetic field conditions, *J. Geophys.*
1294 *Res.*, **112**, A02202, doi:[10.1029/2006JA011877](https://doi.org/10.1029/2006JA011877).
- 1295 Dunlop, M. W., et al. (2011), Magnetopause reconnection across wide local time, *Ann.*
1296 *Geophys.*, **29**, 1683–1697, doi:[10.5194/angeo-29-1683-2011](https://doi.org/10.5194/angeo-29-1683-2011).
- 1297 Elphic, R. C., M. Lockwood, S. W. H. Cowley, and P. E. Sandholt (1990), Flux transfer events at
1298 the magnetopause and in the ionosphere, *Geophys. Res. Lett.*, **17**, 2241.
- 1299 [Fasel, G. J. \(1995\), Dayside poleward moving auroral forms: A statistical study, *J. Geophys.*](#)
1300 [*Res.*, **100**\(A7\), 11891–11905, doi: 10.1029/95JA00854.](#)
- 1301 Fear, R. C., Milan, S. E., Fazakerley, A. N., Lucek, E. A., Cowley, S. W. H., and Dandouras,
1302 I.(2008), The azimuthal extent of three flux transfer events, *Ann. Geophys.*, **26**, 2353-2369,
1303 <https://doi.org/10.5194/angeo-26-2353-2008>.
- 1304 Fear, R. C., S. E. Milan, E. A. Lucek, S. W. H. Cowley, and A. N. Fazakerley (2010), Mixed
1305 azimuthal scales of flux transfer events, in *The Cluster Active Archive – Studying the Earth's*
1306 *Space Plasma Environment*, *Astrophys. Space Sci. Proc.*, edited by H. Laakso, M. Taylor,
1307 and C. P. Escoubet, pp. 389–398, Springer, Dordrecht, Netherlands, doi:[10.1007/978-90-](https://doi.org/10.1007/978-90-481-3499-1_27)
1308 [481-3499-1_27](https://doi.org/10.1007/978-90-481-3499-1_27).
- 1309 [Fuselier, S. A., H. U. Frey, K. J. Trattner, S. B. Mende, and J. L. Burch \(2002\), Cusp aurora](#)
1310 [dependence on interplanetary magnetic field \$B_z\$, *J. Geophys. Res.*, **107**\(A7\), 1111,](#)
1311 [doi:10.1029/2001JA900165](https://doi.org/10.1029/2001JA900165).

- 1335 [Fuselier, S. A., S. B. Mende, T. E. Moore, H. U. Frey, S. M. Petrinec, E. S. Claflin, and M.](#)
1336 [R. Collier \(2003\), Cusp dynamics and ionospheric outflow, in Magnetospheric Imaging—The](#)
1337 [Image Mission, edited by J. L. Burch, Space Sci. Rev., 109, 285,](#)
1338 [doi:10.1023/B:SPAC.0000007522.71147.b3.](#)
- 1339 [Fuselier, S. A., K. J. Trattner, S. M. Petrinec, C. J. Owen, and H. Rème \(2005\), Computing the](#)
1340 [reconnection rate at the Earth's magnetopause using two spacecraft observations, J. Geophys.](#)
1341 [Res., 110, A06212, doi:10.1029/2004JA010805.](#)
- 1342 [Fuselier, S. A., S. M. Petrinec, and K. J. Trattner \(2010\), Antiparallel magnetic reconnection rates](#)
1343 [at the Earth's magnetopause, J. Geophys. Res., 115, A10207, doi:10.1029/2010JA015302.](#)
- 1344 Glocer, A., J. Dorelli, G. Toth, C. M. Komar, and P. A. Cassak (2016), Separator reconnection at
1345 the magnetopause for predominantly northward and southward IMF: Techniques and
1346 results, *J. Geophys. Res. Space Physics*, 121, 140–156, doi:10.1002/2015JA021417.
- 1347 Goertz, C. K., E. Nielsen, A. Korth, K. H. Glassmeier, C. Haldoupis, P. Hoeg, and D.
1348 Hayward (1985), Observations of a possible ground signature of flux transfer events, *J.*
1349 *Geophys. Res.*, 90(A5), 4069–4078, doi:10.1029/JA090iA05p04069.
- 1350 Gonzalez, W. D., and F. S. Mozer (1974), A quantitative model for the potential resulting from
1351 reconnection with an arbitrary interplanetary magnetic field, *J. Geophys. Res.*, 79(28), 4186–
1352 4194, doi:10.1029/JA079i028p04186.
- 1353 [Gosling, J. T., M. F. Thomsen, S. J. Bame, T. G. Onsager, and C. T. Russell \(1990b\), The electron](#)
1354 [edge of low latitude boundary layer during accelerated flow events, *Geophys. Res.*](#)
1355 [*Lett.*, 17, 1833–1836, doi:10.1029/GL017i011p01833.](#)
- 1356 Greenwald, R. A., et al. (1995), DARN/SuperDARN: A global view of the dynamics of high-
1357 latitude convection, *Space Sci. Rev.*, 71, 761–796.

- 1381 Haerendel, G., G. Paschmann, N. Sckopke, H. Rosenbauer, and P. C. Hedgecock (1978), The
1382 frontside boundary layer of the magnetosphere and the problem of reconnection, *J. Geophys.*
1383 *Res.*, 83(A7), 3195–3216, doi:[10.1029/JA083iA07p03195](https://doi.org/10.1029/JA083iA07p03195).
- 1384 Haldoupis, C. (1989), A review on radio studies of auroral E-region ionospheric irregularities, *Ann.*
1385 *Geophys.*, **7**, 239–258.
- 1386 Hasegawa, H., et al. (2016), Decay of mesoscale flux transfer events during quasi - continuous
1387 spatially extended reconnection at the magnetopause, *Geophys. Res. Lett.*, 43, 4755–4762,
1388 doi:[10.1002/2016GL069225](https://doi.org/10.1002/2016GL069225).
- 1389 Haynes, A. L., and C. E. Parnell (2010), A method for finding three-dimensional magnetic
1390 skeletons, *Phys. Plasmas*, **17**, 092903, doi:[10.1063/1.3467499](https://doi.org/10.1063/1.3467499).
- 1391 Hesse, M., M. Kuznetsova, and J. Birn (2001), Particle-in-cell simulations of three-dimensional
1392 collisionless magnetic reconnection, *J. Geophys. Res.*, 106(A12), 29831–29841,
1393 doi:[10.1029/2001JA000075](https://doi.org/10.1029/2001JA000075).
- 1394 Huba, J. D., and L. I. Rudakov (2002), Three-dimensional Hall magnetic reconnection, *Phys.*
1395 *Plasmas*, 9, 4435.
- 1396 Hudson, P. D. (1970), Discontinuities in an anisotropic plasma and their identification in the
1397 solar wind, *Planet. Space Sci.*, 18, 1611–1622.
- 1398 Jain, N., J. Büchner, S. Dorfman, H. Ji, and A. S. Sharma (2013), Current disruption and its
1399 spreading in collisionless magnetic reconnection, *Phys. Plasmas* 20, 112101.
- 1400 Komar, C. M., P. A. Cassak, J. C. Dorelli, A. Gloer, and M. M. Kuznetsova (2013), Tracing
1401 magnetic separators and their dependence on IMF clock angle in global magnetospheric
1402 simulations, *J. Geophys. Res. Space Physics*, 118, 4998–5007, doi:[10.1002/jgra.50479](https://doi.org/10.1002/jgra.50479).
- 1403 Komar, C. M., R. L. Fermo, and P. A. Cassak (2015), Comparative analysis of dayside magnetic

Formatt

Formatt

Formatt

Formatt

1427 reconnection models in global magnetosphere simulations, *J. Geophys. Res. Space*
1428 *Physics*, **120**, 276–294, doi:[10.1002/2014JA020587](https://doi.org/10.1002/2014JA020587).

1429 Koustov, A. V., D. W. Danskin, R. A. Makarevitch, and J. D. Gorin (2005), On the relationship
1430 between the velocity of E-region HF echoes and E B plasma drift, *Ann. Geophys.*, **23**(2),
1431 pp. 371–378, 0992-7689.

1432 [Kuo, H., C. T. Russell, and G. Le \(1995\), Statistical studies of flux transfer events, *J. Geophys.*](#)
1433 [Res., **100**\(A3\), 3513–3519, doi: 10.1029/94JA02498.](#)

1434 Laitinen, T. V., P. Janhunen, T. I. Pulkkinen, M. Palmroth, and H. E. J. Koskinen (2006), On the
1435 characterization of magnetic reconnection in global MHD simulations, *Ann.*
1436 *Geophys.*, **24**, 3059–3069.

1437 Laitinen, T. V., M. Palmroth, T. I. Pulkkinen, P. Janhunen, and H. E. J.
1438 Koskinen (2007), Continuous reconnection line and pressure-dependent energy conversion
1439 on the magnetopause in a global MHD model, *J. Geophys. Res.*, **112**, A11201,
1440 doi:[10.1029/2007JA012352](https://doi.org/10.1029/2007JA012352).

1441 Lapenta, G., D. Krauss-Varban, H. Karimabadi, J. D. Huba, L. I. Rudakov, and P.
1442 Ricci (2006), Kinetic simulations of X-line expansion in 3D reconnection, *Geophys. Res.*
1443 *Lett.*, **33**, L10102, doi:[10.1029/2005GL025124](https://doi.org/10.1029/2005GL025124).

1444 Lee, L. C., and Z. F. Fu (1985), A theory of magnetic flux transfer at the earth's
1445 magnetopause, *Geophys. Res. Lett.*, **12**, 105.

1446 Lockwood, M., P. E. Sandholt, and S. W. H. Cowley, Dayside auroral activity and momentum
1447 transfer from the solar wind, *Geophys. Res. Lett.*, **16**, 33, 1989.

1448 Lockwood, M., M. F. Smith, Low altitude signatures of the cusp and flux transfer
1449 events, *Geophys. Res. Lett.*, **16**, 879–882, 1989.

Formatt

Formatt

Formatt

Formatt

Formatt

- 1473 Lockwood, M., S. W. H. Cowley, P. E. Sandholt, and R. P. Lepping (1990), The ionospheric
1474 signatures of flux transfer events and solar wind dynamic pressure changes, *J. Geophys.*
1475 *Res.*, 95(A10), 17113–17135, doi:[10.1029/JA095iA10p17113](https://doi.org/10.1029/JA095iA10p17113).
- 1476 Lockwood, M., and M. F. Smith (1994), Low and middle altitude cusp particle signatures for
1477 general magnetopause reconnection rate variations: 1. Theory, *J. Geophys. Res.*, 99(A5),
1478 8531–8553, doi:[10.1029/93JA03399](https://doi.org/10.1029/93JA03399).
- 1479 Lockwood, M., et al. (2001), Co-ordinated Cluster and ground-based instrument observations of
1480 transient changes in the magnetopause boundary layer during an interval of predominantly
1481 northward IMF: Relation to reconnection pulses and FTE signatures, *Ann.*
1482 *Geophys.*, **19**, 1613–1640, doi:[10.5194/angeo-19-1613-2001](https://doi.org/10.5194/angeo-19-1613-2001).
- 1483 Luhmann, J. G., R. J. Walker, C. T. Russell, N. U. Crooker, J. R. Spreiter, and S. S.
1484 Stahara (1984), Patterns of potential magnetic field merging sites on the dayside
1485 magnetopause, *J. Geophys. Res.*, **89**, 1739–1742, doi:[10.1029/JA089iA03p01739](https://doi.org/10.1029/JA089iA03p01739).
- 1486 Lui, A. T. Y., and D. G. Sibeck, Dayside auroral activities and their implications for impulsive
1487 entry processes in the dayside magnetosphere, *J. Atmos. Terr. Phys.*, **53**, 219, 1991.
- 1488 McFadden, J. P., et al. (2008), The THEMIS ESA plasma instrument and in-flight
1489 calibration, *Space Sci. Rev.*, **141**, 277–302.
- 1490 [McWilliams, K. A., T. K. Yeoman, and G. Provan \(2000\), A statistical survey of dayside pulsed](#)
1491 [ionospheric flows as seen by the CUTLASS Finland HF radar, *Ann. Geophys.*, 18, 445–453,
1492 \[doi:10.1007/s00585 - 000 - 0445 - 8.\]\(#\)](#)
- 1493 McWilliams, K. A., T.K. Yeoman, and S.W.H. Cowley (2001a), Two-dimensional electric field
1494 measurements in the ionospheric footprint of a flux transfer event, *Annales Geophysicae*,
1495 18, pp. 1584–1598.

Formate

Formate

Formate

Formate

Formate

First line:
Double, M

Formate

Formate

1519 McWilliams, K. A., T.K. Yeoman, J.B. Sigwarth, L.A. Frank, and M. Brittnacher (2001b), The
1520 dayside ultraviolet aurora and convection responses to a southward turning of the
1521 interplanetary magnetic field, *Annales Geophysicae*, 17, pp. 707–721.

1522 McWilliams, K. A., T.K. Yeoman, D.G. Sibeck, S.E. Milan, G.J. Sofko, T. Nagai, T. Mukai, I.J.
1523 Coleman, T. Hori, and F.J. Rich (2004), Simultaneous observations of magnetopause flux
1524 transfer events and of their associated signatures at ionospheric altitudes, *Annales*
1525 *Geophysicae*, 22, pp. 2181–2199.

1526 Milan, S. E., M. Lester, S. W. H. Cowley, and M. Brittnacher (2000), Convection and auroral
1527 response to a southward turning of the IMF: Polar UVI, CUTLASS, and IMAGE signatures
1528 of transient magnetic flux transfer at the magnetopause, *J. Geophys. Res.*, 105(A7), 15741–
1529 15755, doi:[10.1029/2000JA900022](https://doi.org/10.1029/2000JA900022).

1530 Milan, S. E., S. M. Imber, J. A. Carter, M.-T. Walach, and B. Hubert (2016), What controls the
1531 local time extent of flux transfer events?, *J. Geophys. Res. Space Physics*, 121, 1391–1401,
1532 doi:[10.1002/2015JA022012](https://doi.org/10.1002/2015JA022012).

1533 Moen, J., Carlson, H. C., Milan, S. E., Shumilov, N., Lybekk, B., Sandholt, P. E., and Lester, M.:
1534 On the collocation between dayside auroral activity and coherent HF radar backscatter,
1535 *Ann. Geophys.*, 18, 1531-1549, <https://doi.org/10.1007/s00585-001-1531-2>, 2000.

1536 Moore, T. E., M.-C. Fok, and M. O. Chandler, The dayside reconnection X line, *J. Geophys.*
1537 *Res.*, 107(A10), 1332, doi:[10.1029/2002JA009381](https://doi.org/10.1029/2002JA009381), 2002.

1538 Nakamura, T. K. M., R. Nakamura, A. Alexandrova, Y. Kubota, and T. Nagai (2012), Hall
1539 magnetohydrodynamic effects for three-dimensional magnetic reconnection with finite
1540 width along the direction of the current, *J. Geophys. Res.*, 117, A03220,
1541 doi:[10.1029/2011JA017006](https://doi.org/10.1029/2011JA017006).

Formatt

Formatt

Formatt

Formatt

1565 Neudegg, D. A., T. K. Yeoman, S. W. H. Cowley, G. Provan, G. Haerendel, W. Baumjohann, U.
1566 Auster, K.-H. Fornacon, E. Georgescu, and C. J. Owen (1999), A⁻ flux transfer event
1567 observed at the magnetopause by the Equator-S spacecraft and in the ionosphere by the
1568 CUTLASS HF radar, *Ann. Geophysicae*, **17**, 707.

1569 Neudegg, D. A., et al. (2000), A survey of magnetopause FTEs and associated flow bursts in the
1570 polar ionosphere, *Ann. Geophys.*, **18**, 416.

1571 Nishitani, N., T. Ogawa, M. Pinnock, M. P. Freeman, J. R. Dudeney, J.-P. Villain, K. B.
1572 Baker, N. Sato, H. Yamagishi, and H. Matsumoto (1999), A very large scale flow burst
1573 observed by the SuperDARN radars, *J. Geophys. Res.*, 104(A10), 22469–22486,
1574 doi:[10.1029/1999JA900241](https://doi.org/10.1029/1999JA900241).

1575 Newell, P. T., C.-I. Meng, D. G. Sibeck, and R. Lepping (1989), Some low-altitude cusp
1576 dependencies on the interplanetary magnetic field, *J. Geophys. Res.*, 94(A7), 8921–8927,
1577 doi:[10.1029/JA094iA07p08921](https://doi.org/10.1029/JA094iA07p08921).

1578 [Newell P. T., and Meng C.-I. \(1991\), Ion acceleration at the equatorward edge of the cusp: Low-](#)
1579 [altitude observations of patchy merging, *Geophys. Res. Lett.*, **18**, 1829–1832,](#)
1580 [doi:\[10.1029/91GL02088\]\(https://doi.org/10.1029/91GL02088\).](#)

1581 Newell, P. T., and C. - I. Meng (1994), Ionospheric projections of magnetospheric regions under
1582 low and high solar wind conditions, *J. Geophys. Res.*, 99, 273.

1583 Newell, P. T., S. Wing, and F. J. Rich (2007), Cusp for high and low merging rates, *J. Geophys.*
1584 *Res.*, 112, A09205, doi:[10.1029/2007JA012353](https://doi.org/10.1029/2007JA012353).

1585 Newell, P. T., T. Sotirelis, K. Liou, C. - I. Meng, and F. J. Rich (2007b), A nearly universal solar
1586 wind - magnetosphere coupling function inferred from 10 magnetospheric state variables, *J.*
1587 *Geophys. Res.*, 112, A01206, doi: [10.1029/2006JA012015](https://doi.org/10.1029/2006JA012015).

Formatt

Formatt

Formatt

Formatt

Formatt

Formatt

Formatt

Formatt

1611 Tsyganenko, N. A. (1995), Modeling the Earth's magnetospheric magnetic field confined within
1612 a realistic magnetopause, *J. Geophys. Res.*, 100(A4), 5599–5612, doi:[10.1029/94JA03193](https://doi.org/10.1029/94JA03193).

1613 Oksavik, K., J. Moen, and H. C. Carlson (2004), High-resolution observations of the small-scale
1614 flow pattern associated with a poleward moving auroral form in the cusp, *Geophys. Res.
1615 Lett.*, **31**, L11807, doi:[10.1029/2004GL019838](https://doi.org/10.1029/2004GL019838).

1616 Oksavik, K., J. Moen, H. C. Carlson, R. A. Greenwald, S. E. Milan, M. Lester, W. F. Denig,
1617 and R. J. Barnes (2005), Multi-instrument mapping of the small-scale flow dynamics related
1618 to a cusp auroral transient, *Ann. Geophys.*, **23**, 2657–2670.

1619 Paschmann, G., et al. (1979), Plasma acceleration at the Earth's magnetopause: Evidence for
1620 magnetic reconnection, *Nature*, 282, 243.

1621 Paschmann, G., et al. (1986), The magnetopause for large magnetic shear: AMPTE/IRM
1622 observations, *J. Geophys. Res.*, **91**, 11,099.

1623 [Petrinec, S. M., and S. A. Fuselier \(2003\), On continuous versus discontinuous neutral lines at](#)
1624 [the dayside magnetopause for southward interplanetary magnetic field, *Geophys. Res.*](#)
1625 [Lett.](#), 30(10), 1519, doi:[10.1029/2002GL016565](https://doi.org/10.1029/2002GL016565).

1626 [Phan, T. D., and G. Paschmann \(1996\), Low - latitude dayside magnetopause and boundary](#)
1627 [layer for high magnetic shear: 1. Structure and motion, *J. Geophys. Res.*, 101, 7801–7815,](#)
1628 [doi:\[10.1029/95JA03752\]\(https://doi.org/10.1029/95JA03752\).](#)

1629 Phan, T.-D., et al. (2000), Extended magnetic reconnection at the Earth's magnetopause from
1630 detection of bi-directional jets, *Nature*, **404**, 848.

1631 [Phan, T.D., Freeman, M.P., Kistler, L.M. et al, Evidence for an extended reconnection line at the](#)
1632 [dayside magnetopause, *Earth Planet Sp* \(2001\) 53: 619,](#)
1633 <https://doi.org/10.1186/BF03353281>.

Formatte

Formatte

Formatte

Formatte
line: -2 c
defined, S
widow/or

Formatte

Formatte

Formatte

Formatte

Formatte

Formatte

1657 [Phan, T., et al. \(2003\), Simultaneous Cluster and IMAGE observations of cusp reconnection and](#)
1658 [auroral proton spot for northward IMF, *Geophys. Res. Lett.*, 30\(10\), 1509,](#)
1659 [doi:10.1029/2003GL016885.](#)

1660 Phan, T. D., H. Hasegawa, M. Fujimoto, M. Oieroset, T. Mukai, R. P. Lin, and W. R.
1661 Paterson (2006), Simultaneous Geotail and Wind observations of reconnection at the
1662 subsolar and tail flank magnetopause, *Geophys. Res. Lett.*, 33, L09104,
1663 doi:10.1029/2006GL025756.

1664 Phan, T. D., G. Paschmann, J. T. Gosling, M. Oieroset, M. Fujimoto, J. F. Drake, and V.
1665 Angelopoulos (2013), The dependence of magnetic reconnection on plasma β and magnetic
1666 shear: Evidence from magnetopause observations, *Geophys. Res. Lett.*, 40, 11–16,
1667 doi:10.1029/2012GL054528.

1668 Pinnock, M., Rodger, A. S., Dudeney, J. R., Baker, K. B., Newell, P. T., Greenwald, R. A., and
1669 Greenspan, M. E. (1993): Observations of an enhanced convection channel in the cusp
1670 ionosphere, *J. Geophys. Res.*, 98, 3767–3776.

1671 Pinnock, M., A. S. Rodger, J. R. Dudeney, F. Rich, and K. B. Baker (1995), High spatial and
1672 temporal resolution observations of the ionospheric cusps, *Ann. Geophys.*, **13**, 919–925.

1673 Pinnock, M & Rodger, A. (2001). On determining the noon polar cap boundary from
1674 SuperDARN HF radar backscatter characteristics. *Annales Geophysicae*. 18.
1675 10.1007/s00585-001-1523-2.

1676 [Pinnock, M., G. Chisham, I. J. Coleman, M. P. Freeman, M. Hairston, and J.-P. Villain \(2003\),](#)
1677 [The location and rate of dayside reconnection during an interval of southward interplanetary](#)
1678 [magnetic field, *Ann. Geophys.*, 21, 1467–1482.](#)

1679 [Plaschke F, Hietala H. Angelopoulos V. Anti-sunward high-speed jets in the subsolar](#)

1703 [magnetosheath. Ann. Geophys. 2013;31:1877–1889. doi:10.5194/angeo-31-1877-2013.](#)

1704 [Ponomarenko, P. V., Waters, C. L., and Menk, F. W.: Factors determining spectral width of HF](#)

1705 [echoes from high latitudes, Ann. Geophys., 25, 675-687, https://doi.org/10.5194/angeo-25-](#)

1706 [675-2007, 2007.](#)

1707 Provan, G. & Yeoman, T.K. (1999), Statistical observations of the MLT, latitude and size of

1708 pulsed ionospheric flows with the CUTLASS Finland radar, *Annales Geophysicae*, 17:

1709 855. <https://doi.org/10.1007/s00585-999-0855-1>

1710 Provan, G., T. K. Yeoman, and S. E. Milan (1998), CUTLASS Finland radar observations of the

1711 ionospheric signatures of flux transfer events and the resulting plasma flows, *Ann.*

1712 *Geophys.*, **16**, 1411–1422.

1713 Ruohoniemi, J. M., R. A. Greenwald, K. B. Baker, J.-P. Villain, C. Hanuise, and J.

1714 Kelly (1989), Mapping high-latitude plasma convection with coherent HF radars, *J.*

1715 *Geophys. Res.*, 94(A10), 13463–13477, doi:[10.1029/JA094iA10p13463](https://doi.org/10.1029/JA094iA10p13463).

1716 Ruohoniemi, J. M., and K. B. Baker (1998), Large-scale imaging of high-latitude convection

1717 with Super Dual Auroral Radar Network HF radar observations, *J. Geophys.*

1718 *Res.*, 103(A9), 20797–20811, doi:[10.1029/98JA01288](https://doi.org/10.1029/98JA01288).

1719 Russell, C. T., and R. C. Elphic (1979), ISEE observations of flux transfer events at the dayside

1720 magnetopause, *Geophys. Res. Lett.*, 6(1), 33–36, doi:[10.1029/GL006i001p00033](https://doi.org/10.1029/GL006i001p00033).

1721 Sandholt, P. E., C. S. Deehr, A. Egeland, B. Lybekk, R. Viereck, and G. J.

1722 Romick (1986), Signatures in the dayside aurora of plasma transfer from the

1723 magnetosheath, *J. Geophys. Res.*, 91(A9), 10063–10079, doi:[10.1029/JA091iA09p10063](https://doi.org/10.1029/JA091iA09p10063).

1724 Sandholt, P. E., M. Lockwood, T. Oguti, S. W. H. Cowley, K. S. C. Freeman, B. Lybekk, A.

1725 Egeland, and D. M. Willis (1990), Midday auroral breakup events and related energy and

Formatt
Font col

Formatt

Formatt

Formatt

Formatt

Formatt

- 1749 momentum transfer from the magnetosheath, *J. Geophys. Res.*, 95(A2), 1039–1060,
1750 doi:[10.1029/JA095iA02p01039](https://doi.org/10.1029/JA095iA02p01039).
- 1751 Sandholt, P. E., et al. (1994), Cusp/cleft auroral activity in relation to solar wind dynamic
1752 pressure, interplanetary magnetic field B_z and B_y , *J. Geophys. Res.*, 99(A9), 17323–17342,
1753 doi:[10.1029/94JA00679](https://doi.org/10.1029/94JA00679).
- 1754 Scholer, M. (1988), Magnetic flux transfer at the magnetopause based on single x line bursty
1755 reconnection, *Geophys. Res. Lett.*, **15**, 291.
- 1756 Scholer, M., I. Sidorenko, C. H. Jaroschek, R. A. Treumann, and A. Zeiler (2003), Onset of
1757 collisionless magnetic reconnection in thin current sheets: Three-dimensional particle
1758 simulations, *Phys. Plasmas*, **10**(9), 3521–3527.
- 1759 Shay, M. A., J. F. Drake, M. Swisdak, W. Dorland, and B. N. Rogers (2003), Inherently three
1760 dimensional magnetic reconnection: A mechanism for bursty bulk flows? *Geophys. Res.*
1761 *Lett.*, 30(6), 1345, doi:[10.1029/2002GL016267](https://doi.org/10.1029/2002GL016267).
- 1762 Shepherd, L. S., and P. A. Cassak (2012), Guide field dependence of 3-D X-line spreading
1763 during collisionless magnetic reconnection, *J. Geophys. Res.*, 117, A10101,
1764 doi:[10.1029/2012JA017867](https://doi.org/10.1029/2012JA017867).
- 1765 Smith, M. F.M. Lockwood, S.W.H. Cowley, The statistical cusp: a simple flux transfer event
1766 model, *Planet Space Sci.*, 1992
- 1767 Sonnerup, B. U. Ö., and L. J. Cahill Jr. (1967), Magnetopause structure and attitude from
1768 Explorer 12 observations, *J. Geophys. Res.*, **72**, 171.
- 1769 Sonnerup, B. U. (1974), Magnetopause reconnection rate, *J. Geophys. Res.*, 79(10), 1546–1549,
1770 doi:[10.1029/JA079i010p01546](https://doi.org/10.1029/JA079i010p01546).
- 1771 Southwood, D. J. (1985), Theoretical aspects of ionosphere - magnetosphere - solar wind

1795 coupling, *Adv. Space Res.*, 5(4), 7–14, doi:10.1016/0273 - 1177(85)90110 - 3.

1796 Southwood, D. J. (1987), The ionospheric signature of flux transfer events, *J. Geophys.*

1797 *Res.*, **92**, 3207.

1798 Swisdak, M., and J. F. Drake (2007), Orientation of the reconnection X-line, *Geophys. Res.*

1799 *Lett.*, 34, L11106, doi:[10.1029/2007GL029815](https://doi.org/10.1029/2007GL029815).

1800 Southwood, D. J., C. J. Farrugia, and M. A. Saunders (1988), What are flux transfer events? *Planet.*

1801 *Space Sci.*, **36**, 503.

1802 Thorolfsson, A., J.-C. Cerisier, M. Lockwood, P. E. Sandholt, C. Senior, and M.

1803 Lester (2000), Simultaneous optical and radar signatures of poleward-moving auroral

1804 forms, *Ann. Geophys.*, **18**, 1054.

1805 [Trattner, K. J., S. A. Fuselier, and S. M. Petrinec \(2004\), Location of the reconnection line for](#)

1806 [northward interplanetary magnetic field, *J. Geophys. Res.*, 109, A03219,](#)

1807 [doi:10.1029/2003JA009975.](#)

1808 Trattner, K. J., J. S. Mulcock, S. M. Petrinec, and S. A. Fuselier (2007), Probing the boundary

1809 between antiparallel and component reconnection during southward interplanetary magnetic

1810 field conditions, *J. Geophys. Res.*, 112, A08210, doi:[10.1029/2007JA012270](https://doi.org/10.1029/2007JA012270).

1811 [Trattner, K. J., S. A. Fuselier, S. M. Petrinec, T. K. Yeoman, C. P. Escoubet, and H.](#)

1812 [Reme \(2008\), The reconnection sites of temporal cusp structures, *J. Geophys. Res.*, 113,](#)

1813 [A07S14, doi:10.1029/2007JA012776.](#)

1814 [Trattner, K. J., Burch, J. L., Ergun, R., Eriksson, S., Fuselier, S. A., Giles, B. L., ... Wilder, F. D.](#)

1815 [\(2017\). The MMS dayside magnetic reconnection locations during phase 1 and their relation](#)

1816 [to the predictions of the maximum magnetic shear model. *Journal of Geophysical Research:*](#)

1817 [Space Physics, 122, 11,991–12,005. <https://doi.org/10.1002/2017JA024488>.](#)

1841 [Trenchi, L., M. F. Marcucci, G. Pallocchia, G. Consolini, M. B. Bavassano Cattaneo, A. M. Di](#)
1842 [Lellis, H. Rème, L. Kistler, C. M. Carr, and J. B. Cao \(2008\), Occurrence of reconnection jets](#)
1843 [at the dayside magnetopause: Double star observations, J. Geophys. Res., 113, A07S10,](#)
1844 [doi:10.1029/2007JA012774.](#)

1845 Tsyganenko, N. A., A magnetospheric magnetic field model with a warped tail current sheet,
1846 Planet. Space Sci., 87, 5, 1989

1847 Tsyganenko, N. A. (1995), Modeling the Earth's magnetospheric magnetic field confined within
1848 a realistic magnetopause, J. Geophys. Res., 100(A4), 5599–5612,
1849 doi:[10.1029/94JA03193.](#)

1850 Tsyganenko, N. A. (2002a), A model of the magnetosphere with a dawn-dusk asymmetry, 1,
1851 Mathematical structure, J. Geophys. Res., 107(A8), doi:[10.1029/2001JA000219.](#)

1852 Tsyganenko, N. A. (2002b), A model of the near magnetosphere with a dawn-dusk asymmetry,
1853 2, Parameterization and fitting to observations, J. Geophys. Res., 107(A8),
1854 doi:[10.1029/2001JA000220.](#)

1855 Walsh, B. M., J. C. Foster, P. J. Erickson, and D. G. Sibeck (2014a), Simultaneous ground- and
1856 space-based observations of the plasmaspheric plume and reconnection, *Science*, **343**, 1122–
1857 1125, doi:[10.1126/science.1247212.](#)

1858 Walsh, B. M., T. D. Phan, D. G. Sibeck, and V. M. Souza (2014b), The plasmaspheric plume and
1859 magnetopause reconnection, Geophys. Res. Lett., 41, 223–228, doi:[10.1002/2013GL058802.](#)

1860 Walsh, B. M., C. M. Komar, and Y. Pfau-Kempf (2017), Spacecraft measurements constraining
1861 the spatial extent of a magnetopause reconnection X line, Geophys. Res. Lett., 44, 3038–3046,
1862 doi:[10.1002/2017GL073379.](#)

1863 Wang, Y., et al. (2005), Initial results of high-latitude magnetopause and low-latitude flank flux

Formatt
-2 ch

Formatt

Formatt

Formatt

Formatt

Formatt

Formatt

1887 transfer events from 3 years of Cluster observations, *J. Geophys. Res.*, 110, A11221,
1888 doi:[10.1029/2005JA011150](https://doi.org/10.1029/2005JA011150).

1889 Wang, J., et al. (2007), TC1 and Cluster observation of an FTE on 4 January 2005: A close
1890 conjunction, *Geophys. Res. Lett.*, 34, L03106, doi:[10.1029/2006GL028241](https://doi.org/10.1029/2006GL028241).

1891 Wild, J. A., Cowley, S. W. H., Davies, J. A., Khan, H., Lester, M., Milan, S. E., Provan, G.,
1892 Yeoman, T. K., Balogh, A., Dunlop, M. W., Fornacon, K.-H., and Georgescu, E. (2001): First
1893 simultaneous observations of flux transfer events at the high-latitude magnetopause by the
1894 Cluster spacecraft and pulsed radar signatures in the conjugate ionosphere by the CUTLASS
1895 and EISCAT radars, *Ann. Geophys.*, 19, 1491–1508.

1896 Wild, J. A., Milan, S. E., Davies, J. A., Cowley, S. W. H., Carr, C. M., and Balogh, A. (2005):
1897 Double Star, Cluster, and groundbased observations of magnetic reconnection during an
1898 interval of duskward oriented IMF: preliminary results, *Ann. Geophys.*, 23, 2903–2907

1899 Wild, J. A., Milan, S. E., Davies, J. A., Dunlop, M. W., Wright, D. M., Carr, C. M., Balogh, A.,
1900 Reme, H., Fazakerley, A. N., and Marchaudon, A. (2007): On the location of dayside
1901 magnetic reconnection during an interval of duskward oriented IMF, *Ann. Geophys.*, 25, 219–
1902 238.

1903 Zhang, Q.-H., et al. (2008), Simultaneous tracking of reconnected flux tubes: Cluster and
1904 conjugate SuperDARN observations on 1 April 2004, *Ann. Geophys.*, **26**, 1545–1557,
1905 doi:[10.5194/angeo-26-1545-2008](https://doi.org/10.5194/angeo-26-1545-2008).

1906 Zou, Y., Walsh, B. M., Nishimura, Y., Angelopoulos, V., Ruohoniemi, J. M., McWilliams, K.
1907 A., & Nishitani, N. (2018). Spreading speed of magnetopause reconnection X-lines using
1908 ground-satellite coordination. *Geophysical Research Letters*, 45.
1909 <https://doi.org/10.1002/2017GL075765>

Formatt

Formatt

Formatt

Formatt

1933
1934
1935
1936
1937
1938
1939
1940
1941
1942
1943
1944
1945
1946
1947
1948
1949
1950
1951
1952
1953
1954
1955

Formatt
Formatt
After: 0 p
Formatt

Figure 1a: OMNI IMF condition on Feb 2, 2013. Figure 1b: THE and THA locations projected to the GSM X-Y plane. The inner curve marks the magnetopause and the outer curve marks the bow shock.

Figure 2a: SuperDARN LOS speeds (color tiles) and merged velocity vectors (color arrows) in the Altitude adjusted corrected geomagnetic (AACGM) coordinates. The FOVs of the RKN, INV, and CLY radars are outlined with the black dashed lines. The colors of the tiles indicate the LOS speeds away from the radar. The colors and the lengths of the arrows indicate the merged velocity magnitudes and the arrow directions indicate the velocity directions. Red and anti-sunward directed flows are the ionospheric signature of magnetopause reconnection. The dashed magenta lines mark the flow western and eastern boundaries. The open-closed field line boundary was delineated by the dashed black curve marked by the “OCB” marker. The satellite footprints under the T89 are shown as the THE and THA marker. Figure 2b: Similar to Figure 2a but showing SECS velocity vectors (color arrows). Figure 2c: Similar to Figure 2a but showing SHF velocity vectors (color arrows). Figure 2d: SuperDARN spectral width measurements (color tiles). The red

1956 contour marks localized enhanced soft electron precipitation. Figure 2e: Time evolution of INV
1957 LOS velocities along 80° MLAT. The velocities are color coded in the same way as Figure 2a.
1958 Figure 2f: Longitudinal profile of convection velocities along 80° MLAT at 1925 UT. The profile
1959 is also shown as a function of the distance measured azimuthally from 0° MLON. The profile in
1960 black is based on the LOS measurements and the profile in red is the northward component of the
1961 SECS velocities. The FWHM is determined based on each profile. Figures 2g-j: THE measured
1962 magnetic field (0.25 s resolution), ion energy flux (3 s), ion density (3 s), and ion velocity (3 s).
1963 The ion measurements were taken from ground ESA moments. The magnetic field and the ion
1964 velocity components are displayed in the LMN boundary normal coordinate system. The
1965 magnetopause crossing is shaded in pink. Figure 2k: THE ion distribution function on the bulk
1966 velocity-magnetic field plane. The small black line indicates the direction and the bulk velocity of
1967 the distributions. Figures 2l-p: THA measurements in the same format as in Figures 2g-k. Figures
1968 2q-z: THA and THE measurements during a subsequent magnetopause crossing shown in the same
1969 format as in Figures 2g-p.
1970
1971 Figure 3: OMNI IMF condition and THEMIS satellite locations on Apr 19, 2015 in a similar format
1972 to Figure 1.
1973
1974 Figure 4. THEMIS and SuperDARN measurements of reconnection bursts on Apr 19, 2015 in a
1975 similar format to Figure 2. The velocity time evolution in Figure 4e and the velocity profile in
1976 Figure 4f are taken along 79 °MLAT.
1977
1978 Figure 5. OMNI IMF condition and THEMIS satellite locations on Apr 29, 2015 in a similar format

1979 to Figure 1.

1980

1981 Figures 6a-d: SuperDARN measurements of reconnection bursts on Apr 29, 2015 in a similar

1982 format to Figures 2a-d except that in Figure 6a the color of the CLY color tiles represent LOS

1983 speeds towards the radar as here LOS speeds towards the CLY radar project to the anti-sunward

1984 direction. Figures 6e-f: Time evolution of LOS velocities along 80° MLAT from the INV and CLY

1985 radars. The velocity measurements in the shaded region are backscatters from the E-region

1986 ionosphere and thus underestimate the convection speed. The flow channel spread azimuthally

1987 before reaching an extended extent, and the time-dependent locations of its western and eastern

1988 boundaries are marked by the dashed magenta lines. Figures 6g-h: Longitudinal profiles of the

1989 LOS and the poleward SECS velocities along 80° MLAT when THA and THE observed

1990 reconnection. Figures 6i-r: THEMIS measurements of reconnection bursts in a similar format to

1991 Figures 2g-p, but the magnetic field and plasma velocities are displayed in the GSM coordinates.

1992

1993 ~~Figure 1. Measurements from THD and THA during their nearly simultaneous crossings of the~~

1994 ~~magnetopause on March 11, 2014. Figure 1a: OMNI IMF condition. Figure 1b: THD and THA~~

1995 ~~locations projected to the GSM X-Y plane. The dashed curve marks the magnetopause and the~~

1996 ~~dotted curve marks the bow shock. Figures 1c-f: THD measured magnetic field (0.25 s resolution),~~

1997 ~~ion energy flux (3 s), ion density (3 s), and ion velocity (3 s). The ion measurements were taken~~

1998 ~~from ground ESA moments. The magnetic field and the ion velocity components are displayed in~~

1999 ~~the LMN boundary normal coordinate system. The magnetopause crossing is shaded in pink.~~

2000 ~~Figure 1g: THD ion distribution function on the bulk velocity-magnetic field plane. The small~~

2001 ~~black line indicates the direction and the bulk velocity of the distributions. Figures 1h-l: THA~~

2002 ~~measurements in the same format as in Figures 1c-g.~~

2003

2004 ~~Figure 2. Ionospheric velocity field at the cusp when the THEMIS satellites crossed the~~

2005 ~~magnetopause on March 11, 2014. Figure 2a: SuperDARN LOS speeds (color tiles) and merged~~

2006 ~~velocity vectors (color arrows) in the Altitude adjusted corrected geomagnetic (AACGM)~~

2007 ~~coordinates. The FOVs of the RKN, INV, and CLY radars are outlined with the black dashed lines.~~

2008 ~~The colors of the tiles indicate the LOS speeds away from the radar. The colors and the lengths of~~

2009 ~~the arrows indicate the merged velocity magnitudes and the arrow directions indicate the velocity~~

2010 ~~directions. Red and anti-sunward directed flows are the ionospheric signature of magnetopause~~

2011 ~~reconnection. The dashed magenta lines mark the flow western and eastern boundaries. The~~

2012 ~~satellite footprints under the T89 are shown as the THD and THA marker. Figure 2b: Similar to~~

2013 ~~Figure 2a but showing SECS velocity vectors (color arrows). Figure 2c: Similar to Figure 2a but~~

2014 ~~showing SHF velocity vectors (color arrows). Figure 2d: SuperDARN spectral width~~

2015 ~~measurements (color tiles). The red contour marks the cusp. Figure 2e: Time evolution of RKN~~

2016 ~~LOS velocities along 80° MLAT. The velocities are color coded in the same way as Figure 2a.~~

2017 ~~Figure 2f: Longitudinal profile of convection velocities along 80° MLAT at 1622 UT. The profiles~~

2018 ~~is also shown as a function of the distance measured azimuthally from 0° MLON. The profile in~~

2019 ~~black is based on the RKN LOS measurements, from which the HWHM is determined and marked~~

2020 ~~by the black arrow. The profile in red is based on the northward components of the SECS velocities,~~

2021 ~~from which the FWHM is determined and marked by the red arrow. The dotted black and red~~

2022 ~~vertical lines are the drop lines of the HWHM and FWHM, respectively.~~

2023

2024 ~~Figure 3. Measurements from THA and THE during their nearly simultaneous crossings of the~~

2025 magnetopause on Apr 19, 2015. The figure format is similar to Figure 1.

2026

2027 ~~Figure 4. Ionospheric velocity field at the cusp when the THEMIS satellites crossed the~~
2028 ~~magnetopause on Apr 19, 2015. The figure format is similar to Figure 2. The velocity time~~
2029 ~~evolution in Figure 4e and the velocity profile in Figure 4f are taken along 79° MLAT.~~

2030

2031 ~~Figure 5. Measurements from THA and THE during their crossings of the magnetopause on Apr~~
2032 ~~29, 2015. The figure format is similar to Figure 1, but the magnetic field and plasma velocities are~~
2033 ~~displayed in the GSM coordinates.~~

2034

2035 ~~Figure 6. Figures 6a-d: Ionospheric velocity field at the cusp when the THEMIS satellites crossed~~
2036 ~~the magnetopause on Apr 29, 2015. The figure format is similar to Figures 2a-d except that in~~
2037 ~~Figure 6a the color of the CLY color tiles represent LOS speeds towards the radar as here LOS~~
2038 ~~speeds towards the CLY radar project to the anti-sunward direction. Figures 6e-f: Time evolution~~
2039 ~~of LOS velocities along 80° MLAT from the INV and CLY radars. The velocity measurements in~~
2040 ~~the shaded region are backscatters from the E-region ionosphere and thus underestimate the~~
2041 ~~convection speed. The flow channel spread azimuthally before reaching an extended extent, and~~
2042 ~~the time-dependent locations of its western and eastern boundaries are marked by the dashed~~
2043 ~~magenta lines. Figures 6g-h: Longitudinal profiles of the LOS and the poleward SECS velocities~~
2044 ~~along 80° MLAT when THA and THE observed reconnection.~~

2045

2046 Figure 7. Comparison of the IMF and solar wind driving conditions between the reconnection
2047 events on Feb 2, 2013 ~~March 11, 2014~~, Apr 19, 2015, and Apr 29, 2015. From top to bottom: IMF

2048 in GSM coordinates, solar wind speed, and solar wind dynamic pressure. The red vertical lines
2049 mark the times of the satellite-ground conjunction.

2050

2051

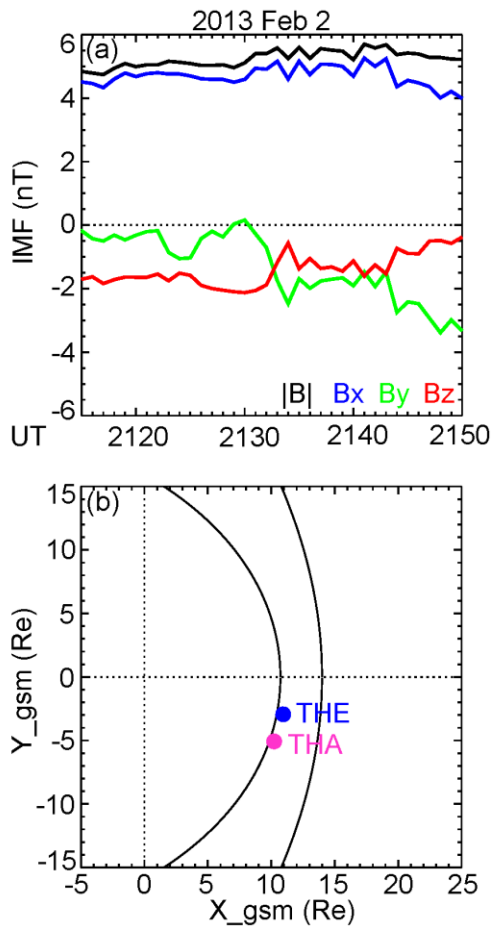
2052

2053

2054

2055

2056 Figure 1.



2057

2058

2059

2060

2061

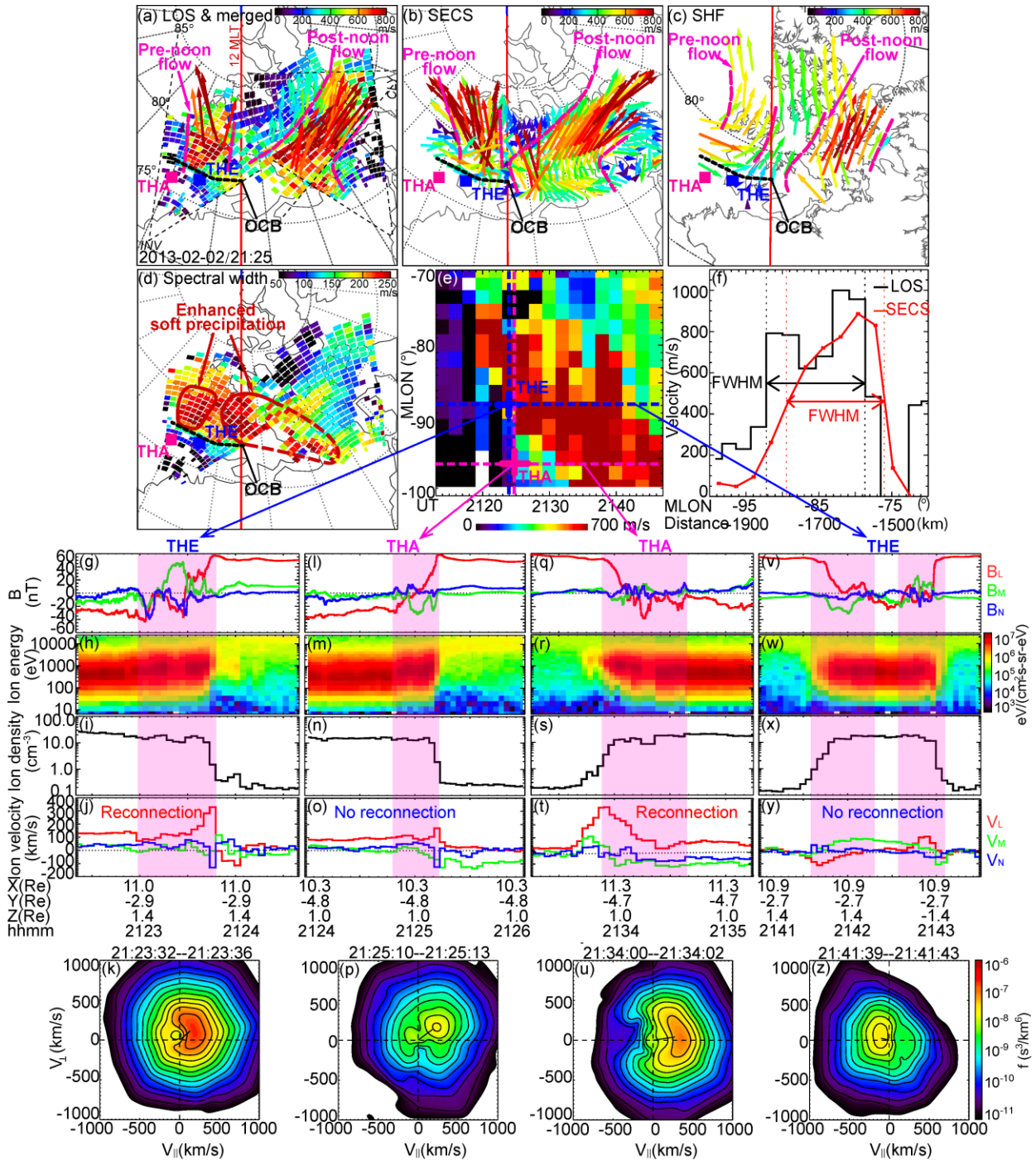
2062

2063

2064

2065

2066



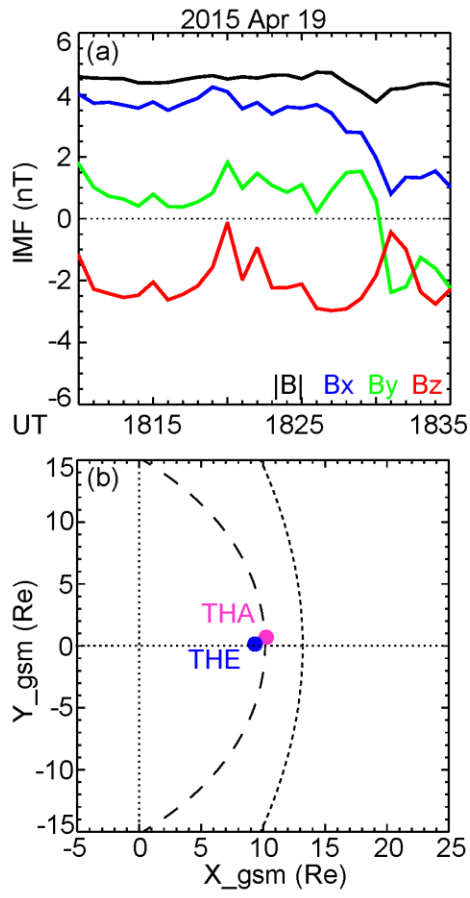
2068

2069

2070

2071

2072 Figure 3,



2073

2074

2075

2076

2077

2078

2079

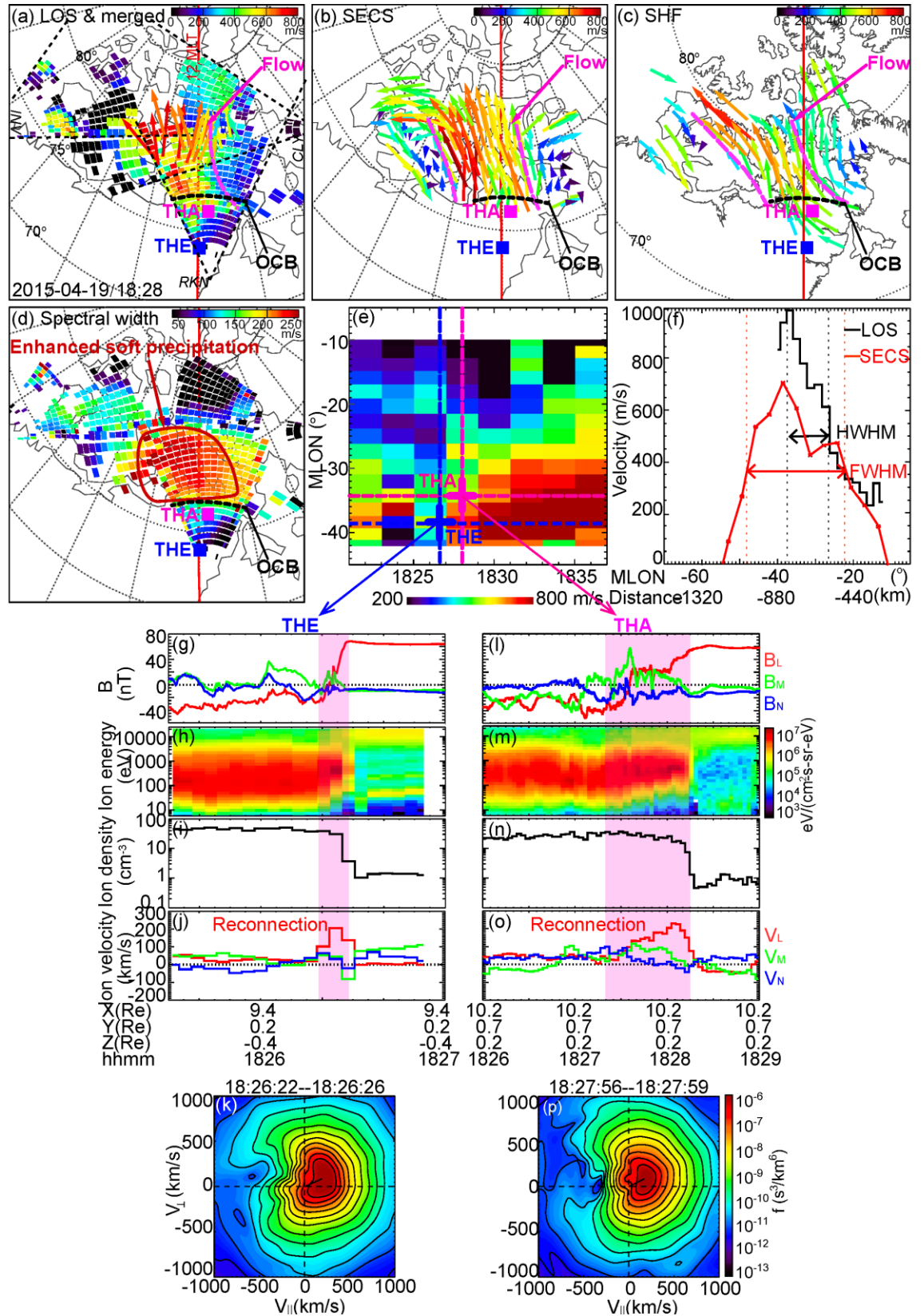
2080

2081

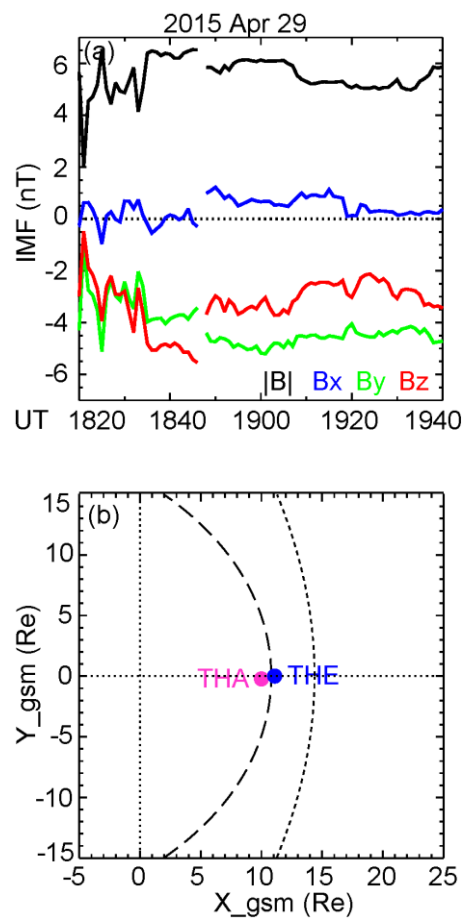
2082

2083

2084 Figure 4.



2085 Figure 5.



2086

2087

2088

2089

2090

2091

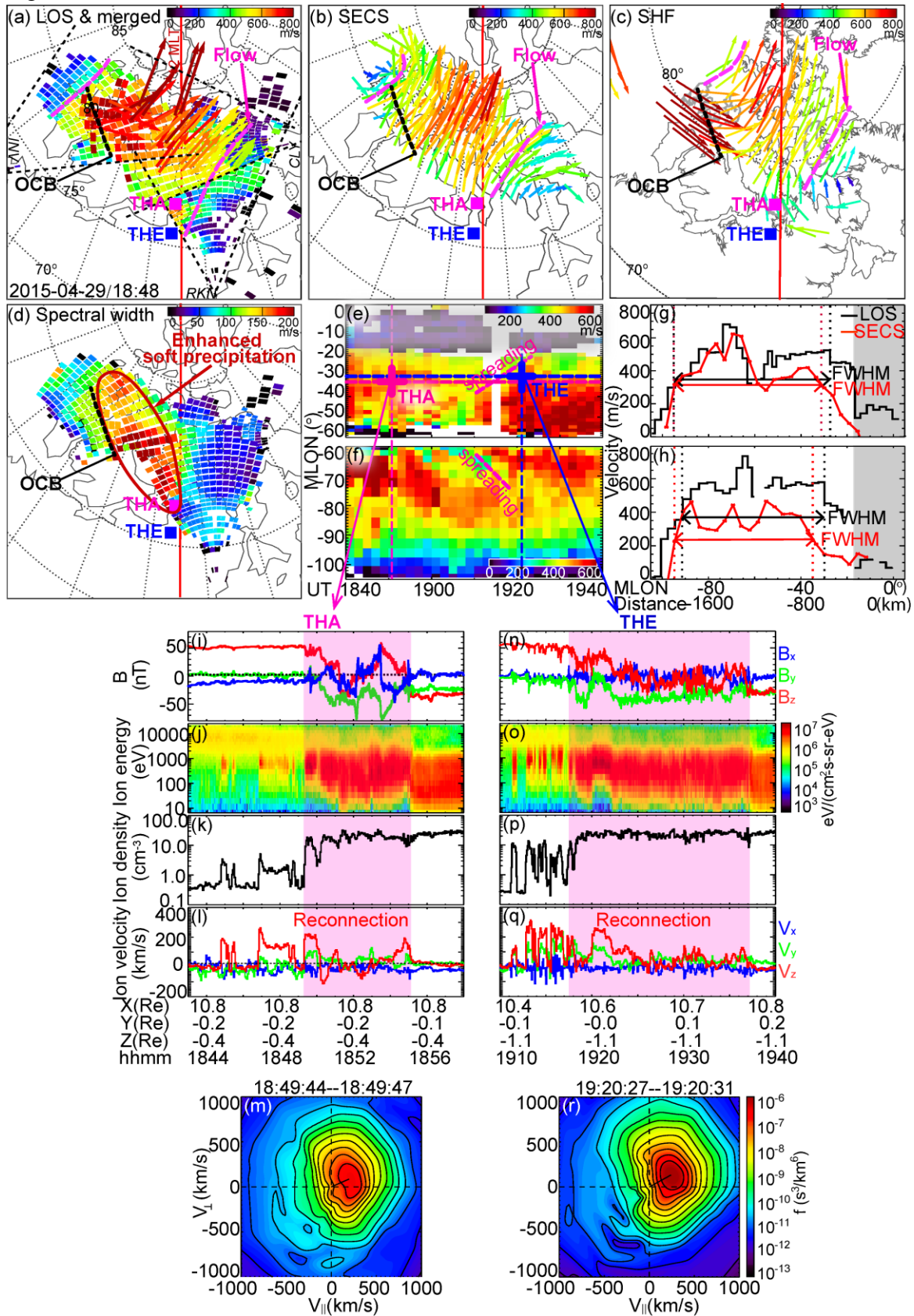
2092

2093

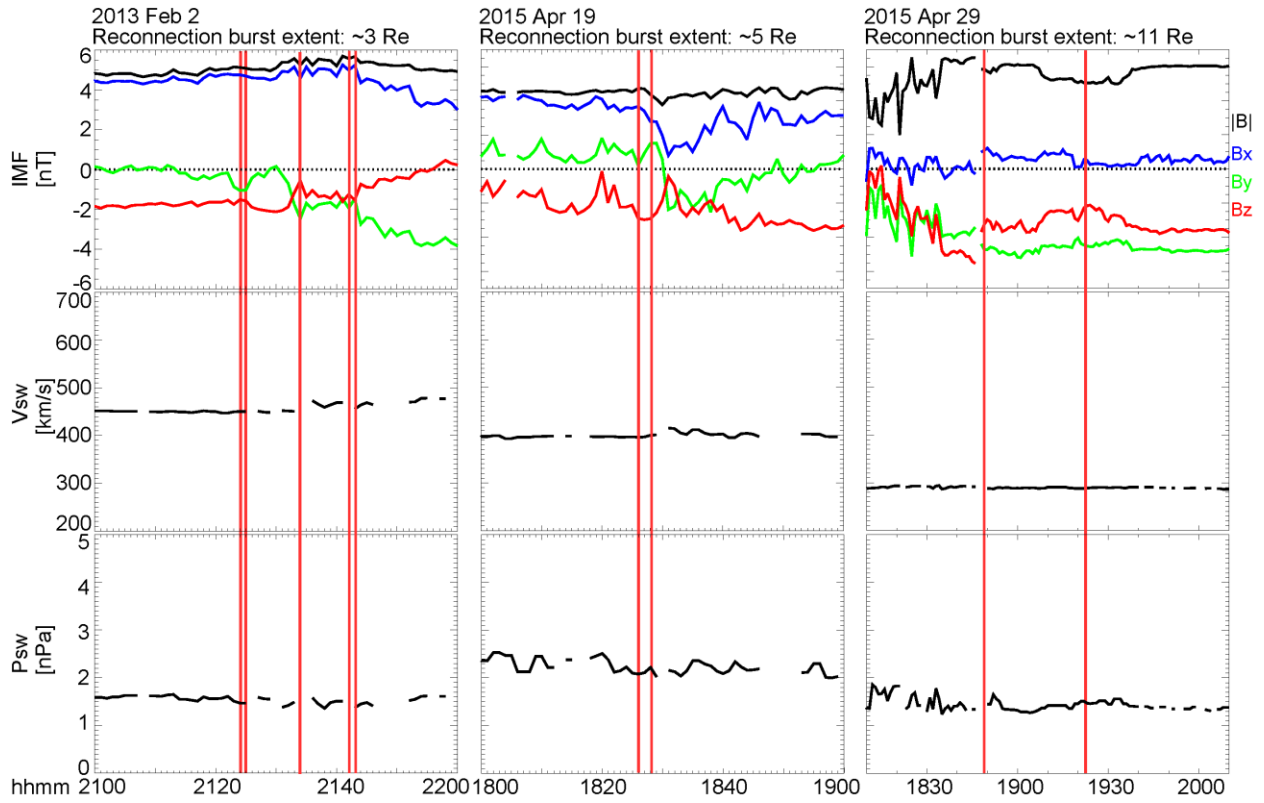
2094

2095

2096 Figure 6.



2097 Figure 7.



2098

2099

2100

2101

2102

2103

2104

2105

2106

2107

2108

2109